

# 5'-tRNA<sup>Gly(GCC)</sup> halves generated by IRE1 $\alpha$ are linked to the ER stress response

Received: 31 October 2023

Accepted: 16 October 2024

Published online: 28 October 2024

Check for updates

Hanyong Jin<sup>1,6</sup>, Ji-Hyun Yeom<sup>2,3,6</sup>, Eunyoung Shin<sup>2,4,6</sup>, Yoonjie Ha<sup>2,6</sup>, Haifeng Liu<sup>5,6</sup>, Daeyoung Kim<sup>2,6</sup>, Minju Joo<sup>2,3,6</sup>, Yong-Hak Kim<sup>4,6</sup>, Hak Kyun Kim<sup>2,6</sup>, Minkyung Ryu<sup>2,3,6</sup>, Hong-Man Kim<sup>3,6</sup>, Jeongkyu Kim<sup>2</sup>, Keun P. Kim<sup>2</sup>, Yoonsoo Hahn<sup>2</sup>, Jeehyeon Bae<sup>5</sup> & Kangseok Lee<sup>2,3</sup>

Transfer RNA halves (tRHs) have various biological functions. However, the biogenesis of specific 5'-tRHs under certain conditions remains unknown. Here, we report that inositol-requiring enzyme 1 $\alpha$  (IRE1 $\alpha$ ) cleaves the anticodon stem-loop region of tRNA<sup>Gly(GCC)</sup> to produce 5'-tRHs (5'-tRH-Gly<sup>GCC</sup>) with highly selective target discrimination upon endoplasmic reticulum (ER) stress. Levels of 5'-tRH-Gly<sup>GCC</sup> positively affect cancer cell proliferation and modulate mRNA isoform biogenesis both in vitro and in vivo; these effects require co-expression of two nuclear ribonucleoproteins, HNRNPM and HNRNPH2, which we identify as binding proteins of 5'-tRH-Gly<sup>GCC</sup>. In addition, under ER stress in vivo, we observe simultaneous induction of IRE1 $\alpha$  and 5'-tRH-Gly<sup>GCC</sup> expression in mouse organs and a distantly related organism, *Cryptococcus neoformans*. Thus, collectively, our findings indicate an evolutionarily conserved function for IRE1 $\alpha$ -generated 5'-tRH-Gly<sup>GCC</sup> in cellular adaptation upon ER stress.

Transfer RNA-derived fragments (tRFs) or transfer RNA-derived small RNAs (tsRNAs) have been recognised as functional small non-coding RNAs (ncRNAs) present in most organisms<sup>1</sup>. Multiple classes of tRFs have been identified in various cell types. In particular, 31–40 nucleotide (nt) long tRFs generated by specific cleavage in the anticodon loop of mature tRNAs are referred to as tRNA halves (tRHs)<sup>1</sup>. Other tRFs are 14–40 nt in length and primarily correspond to the ends of mature tRNA (5'-tRFs and 3'-CCA tRFs) or pre-tRNA (3'-U tRFs)<sup>1</sup>.

In mammalian cells, limited information exists regarding the enzymes that generate tRFs. Angiogenin (ANG), a member of the RNase A superfamily, produces tRHs under certain stress conditions<sup>2–5</sup>. In the case of RNase Z, it cleaves pre-tRNAs and generates 3'-U tRFs containing a stretch of U residues<sup>6</sup>. Additionally, Dicer induces cleavage in the D loop and T loop of tRNAs, producing 5'-tRFs and 3'-CCA tRFs, respectively<sup>7,8</sup>. Furthermore, recent deep

sequencing data suggest that dicer processes tRFs in specific tRNAs and cell types<sup>9</sup>.

Functional roles of identified tRFs in biological processes include translational regulation of gene expression<sup>10–13</sup>, gene silencing, and regulation of ribosome synthesis<sup>6,14</sup>. tRHs affect cell proliferation<sup>4,14–18</sup>, apoptosis<sup>5</sup>, and epigenetic inheritance<sup>19,20</sup>. In mice, changes in the profiles of a subset of sperm tRFs, including 5'-tRHs of tRNA<sup>Gly(GCC)</sup> (5'-tRH-Gly<sup>GCC</sup>), were reported with a high-fat diet<sup>19</sup> and protein restriction increases 5'-tRH-Gly<sup>GCC</sup> levels<sup>20</sup>. In human cancer, 5'-tRH-Gly<sup>GCC</sup>, induced by alkB homologue 3,  $\alpha$ -ketoglutarate dependent dioxygenase (ALKBH3)—a tRNA demethylase—benefits the growth and progression of cervical carcinoma<sup>16</sup> and upregulated 5'-tRH-Gly<sup>GCC</sup> levels were observed in papillary thyroid carcinoma<sup>18</sup>. Although 5'-tRH-Gly<sup>GCC</sup> appears to play various roles in cellular physiology, it remains unclear which enzyme generates these tRHs.

<sup>1</sup>Key Laboratory of Natural Medicines of the Changbai Mountain, Ministry of Education, College of Pharmacy, Yanbian University, Yanji 133002 Jilin, China.

<sup>2</sup>Department of Life Science, Chung-Ang University, Seoul 06974, Republic of Korea. <sup>3</sup>R & D Institute, NES Biotechnology, Seoul 06974, Republic of Korea.

<sup>4</sup>Department of Microbiology, School of Medicine, Catholic University of Daegu, Daegu 42472, Republic of Korea. <sup>5</sup>School of Pharmacy, Chung-Ang University, Seoul 06974, Republic of Korea. <sup>6</sup>These authors contributed equally: Hanyong Jin, Ji-Hyun Yeom, Eunyoung Shin, Yoonjie Ha, Haifeng Liu,

Daeyoung Kim, Minju Joo, Yong-Hak Kim, Hak Kyun Kim, Minkyung Ryu, Hong-Man Kim. e-mail: [jeehyeon@cau.ac.kr](mailto:jeehyeon@cau.ac.kr); [kangseok@cau.ac.kr](mailto:kangseok@cau.ac.kr)

A structural analysis of inositol-requiring enzyme 1 $\alpha$  (IRE1 $\alpha$ ) revealed that the catalytic residues of both the tRNA endonuclease and IRE1 $\alpha$  contain functional groups with a shared chemical nature and spatial disposition<sup>21</sup>. IRE1 $\alpha$ —a key regulator of signalling in the unfolded protein response (UPR)—is a conserved ER-localised transmembrane protein with ribonuclease activity<sup>22</sup>. Upon ER stress, IRE1 $\alpha$  becomes activated and cleaves specific sites in the mRNA that encodes the transcription factor X-box-binding protein 1 (XBP1)<sup>23,24</sup>. IRE1 $\alpha$  also participates in regulated IRE1 $\alpha$ -dependent decay, i.e., the degradation of multiple mRNAs and miRNAs under ER stress in an XBP1-independent manner<sup>25–27</sup>. In particular, a consensus sequence (5'-CH<sub>(U or A or C)</sub>GCM<sub>(A or C)</sub>R<sub>(G or A)</sub>-3') accompanied by a stem-loop structure was proposed as an IRE1 $\alpha$  cleavage site in mRNA<sup>28</sup>.

Herein, we observed that several tRNAs bear the consensus element for IRE1 $\alpha$  cleavage in their anticodon loop region. Considering that tRNA<sup>Gly(GCC)</sup> is one such tRNA, we hypothesised that IRE1 $\alpha$  may participate in producing 5'-tRFs from tRNA<sup>Gly(GCC)</sup>. To test the hypothesis, we aimed to investigate the direct involvement of IRE1 $\alpha$  in the production of 5'-tRFs from tRNA<sup>Gly(GCC)</sup>, as well as their physiological function under ER stress.

## Results

### 5'-tRF accumulation by IRE1 $\alpha$ upregulation

To explore whether IRE1 $\alpha$  can cleave tRNAs and produce 5'-tRFs, we compared tRF profiles in human ovarian cancer-derived KGN cells endogenously expressing IRE1 $\alpha$  (KGN-WT) with those in the same cells exogenously overproducing IRE1 $\alpha$  (KGN-IRE1 $\alpha^{\text{oe}}$ ) by small RNA-sequencing (small RNA-seq). We selected human ovarian cancer cells, as 5'-tRF-Gly<sup>GCC</sup> reportedly functions in reproductive cells<sup>16,19,29</sup>. The relative abundance of 5'-tRFs from tRNA<sup>Gly(GCC)</sup> species markedly increased when IRE1 $\alpha$  was overexpressed (Fig. 1a and Supplementary Table 1). Additionally, 5'-tRFs from tRNA<sup>Cys(GCA)</sup> appeared to accumulate, albeit at much lower levels compared to those from tRNA<sup>Gly(GCC)</sup> in KGN-IRE1 $\alpha^{\text{oe}}$  cells (Fig. 1a and Supplementary Table 1). These results support the notion that among tRNA species, only tRNA<sup>Gly(GCC)</sup> and tRNA<sup>Cys(GCA)</sup> bear the consensus element for IRE1 $\alpha$  cleavage in their anticodon stem-loop region.

Among three different tRNA<sup>Gly</sup> isoacceptors, containing GCC, UCC, and CCC anticodons, 5'-tRFs with their 3'-end corresponding to position 33 of tRNA<sup>Gly(GCC)</sup> were most abundant and enriched in KGN-IRE1 $\alpha^{\text{oe}}$  compared to KGN cells (Fig. 1a and Supplementary Table 1). In addition, high levels of 5'-tRFs, with their 3'-end corresponding to positions 31 and 32 of tRNA<sup>Gly(GCC)</sup>, were observed when IRE1 $\alpha$  was overexpressed (Fig. 1a, b, and Supplementary Table 1). These 5'-tRFs from tRNA<sup>Gly(GCC)</sup> occupied approximately 66% of the total 5'-tRFs from IRE1 $\alpha^{\text{oe}}$  cells (Fig. 1b), indicating that IRE1 $\alpha$  overexpression primarily generates 5'-tRFs from tRNA<sup>Gly(GCC)</sup>. In the case of tRNA<sup>Cys(GCA)</sup>, high levels of 5'-tRFs, with their 3'-end corresponding to positions 33 and 34 (-8% and -1%, respectively), were observed when IRE1 $\alpha$  was overexpressed (Fig. 1a, b, and Supplementary Table 1). We also observed enrichment of 5'-tRFs with their 3'-end corresponding to position 33 of tRNA<sup>Gly(CCC)</sup> in IRE1 $\alpha$ -overexpressing cells; however, these 5'-tRFs accounted for only ~3% of the total (Fig. 1a, b, and Supplementary Table 1).

To validate the small RNA-seq results, tRNA fragments were analysed via northern blotting with specific probes for the 5' upstream regions of the tRNA<sup>Gly(GCC)</sup>, tRNA<sup>Lys(CTT)</sup>, tRNA<sup>Cys(GCA)</sup>, and tRNA<sup>Gly(TCC)</sup> anticodon stem-loops. An IRE1 $\alpha$  expression-dependent increase was observed in the levels of 5'-tRFs from tRNA<sup>Gly(GCC)</sup> and tRNA<sup>Cys(GCA)</sup> (Fig. 1c). The relative abundances of these 5'-tRFs were -1.2% and -0.1% of full-length tRNA<sup>Gly(GCC)</sup> and tRNA<sup>Cys(GCA)</sup>, respectively. The length of these 5'-tRFs corresponded to 32 and 33 nt-long synthetic RNAs containing sequences of 5'-tRFs from tRNA<sup>Gly(GCC)</sup> (Fig. 1c). The relative abundances of other 5'-tRFs from tRNA<sup>Gly(TCC)</sup> and tRNA<sup>Lys(CTT)</sup> were not significantly changed upon IRE1 $\alpha$  overexpression, which agreed with

the small RNA-seq results. Moreover, overexpression of a catalytically inactive form of IRE1 $\alpha$  (K599A)<sup>30</sup> did not significantly impact the levels of these 5'-tRFs (Supplementary Fig. 1), indicating IRE1 $\alpha$  cleavage activity-dependent production of 5'-tRF-Gly<sup>GCC</sup>.

To assess the size of tRFs from tRNA<sup>Gly(GCC)</sup>, we performed primer extension analysis on the samples used for northern blot analysis. Primer extension targeting for tRNA<sup>Gly(GCC)</sup> produced one distinct cDNA band in reactions prepared with RNA samples from KGN-IRE1 $\alpha^{\text{oe}}$  cells. This cDNA band was synthesised from the 3'-tRF of tRNA<sup>Gly(GCC)</sup>, whose 5'-end corresponded to position 34 (Fig. 1d). This 3'-tRF of tRNA<sup>Gly(GCC)</sup> can be generated by IRE1 $\alpha$  cleavage of tRNA<sup>Gly(GCC)</sup> between positions 33 and 34 within its anticodon stem-loop region (C<sup>31</sup>UG  $\downarrow$  CCAC<sup>37</sup>). This cleavage can also generate a 33-nt long 5'-tRF of tRNA<sup>Gly(GCC)</sup>, with the same 3'-end that mapped the highest in KGN-IRE1 $\alpha^{\text{oe}}$  cells in small RNA-seq analysis (Fig. 1a, b). We were not able to detect cDNA bands corresponding 31 and 32 nt-long tRFs that were indicated in small RNA-seq and northern blot analyses (Fig. 1a–c). Collectively, these results indicate that IRE1 $\alpha$  activity is primarily responsible for generation of 5'-tRFs from tRNA<sup>Gly(GCC)</sup>.

### Selective cleavage of tRNA<sup>Gly(GCC)</sup> by IRE1 $\alpha$

To assess whether IRE1 $\alpha$  is solely responsible for the production of 5'-tRFs from tRNA<sup>Gly(GCC)</sup>, we isolated tRNAs from KGN cell total RNA by size fractionation. Purified tRNAs were then incubated with human IRE1 $\alpha$ . IRE1 $\alpha$  was found to selectively cleave tRNA<sup>Gly(GCC)</sup> in vitro (Fig. 2a). Specifically, IRE1 $\alpha$ -mediated cleavage of tRNA<sup>Gly(GCC)</sup> generated one major and two minor 5'-tRNA<sup>Gly(GCC)</sup> fragments (Fig. 2a). When the 3'-end of these fragments was mapped by primer extension analysis, seven distinct cDNA bands (Fig. 2b) were detected. The cDNA band was most prominent and could be synthesised from the 3'-tRF of tRNA<sup>Gly(GCC)</sup> with a 5'-end corresponding to position 34 (Fig. 2b, labelled as b). This 3'-tRF could be generated by IRE1 $\alpha$  cleavage of tRNA<sup>Gly(GCC)</sup> between positions 33 and 34 within its anticodon stem-loop region (C<sup>31</sup>UG  $\downarrow$  CCAC<sup>37</sup>). This cleavage site corresponded to the 3'-end of the most abundant 5'-tRFs from tRNA<sup>Gly(GCC)</sup> that were identified by small RNA-seq in Fig. 1a, b. Moreover, this cDNA band is identical to the distinct cDNA detected in the primer extension assay of tRNA<sup>Gly(GCC)</sup> fragments in KGN cells following IRE1 $\alpha$  overexpression (Fig. 1d). Another distinct band (labelled as a) also corresponded to the 3'-end of the second most abundant 5'-tRFs from tRNA<sup>Gly(GCC)</sup> identified in small RNA-seq (Figs. 1a, b, and 2b). Meanwhile, the cleavage sites deduced from other cDNA bands were not observed in the small RNA-seq analysis in Fig. 1a, b, or in the primer extension of in vivo generated fragments of tRNA<sup>Gly(GCC)</sup> in Fig. 1d.

To further biochemically verify the ability of IRE1 $\alpha$  to cleave tRNA<sup>Gly(GCC)</sup>, we conducted an in vitro IRE1 $\alpha$  cleavage reaction using purified tRNA<sup>Gly(GCC)</sup> as a substrate (Supplementary Fig. 2). Generation of two major and five minor cleavage products appeared to be dependent on IRE1 $\alpha$  (Fig. 2c). Among them, one major cleavage product (labelled as 5) corresponded to an IRE1 $\alpha$  cleavage product of tRNA<sup>Gly(GCC)</sup> between positions 33 and 34 (Fig. 2c). This cleavage site corresponded to the 3'-end of the most abundant 5'-tRFs from tRNA<sup>Gly(GCC)</sup> identified via small RNA-seq in Fig. 1a, b, and was the only cDNA detected in the primer extension assay of tRNA<sup>Gly(GCC)</sup> in vivo generated fragments in Fig. 1d when IRE1 $\alpha$  was overexpressed. Five other products in Fig. 2c also corresponded to IRE1 $\alpha$  cleavage products of tRNA<sup>Gly(GCC)</sup> at sites generated by in vitro IRE1 $\alpha$  cleavage of total tRNAs (Fig. 2b). An additional cleavage product (labelled as 7) in Fig. 2c was also detected in small RNA-seq (Fig. 1a). However, several tRFs identified from in vitro cleavage of tRNA<sup>Gly(GCC)</sup> were not detected in the small RNA-seq analyses (Fig. 1a, b) or primer extension assay of tRNA<sup>Gly(GCC)</sup> fragments generated in vivo (Fig. 1d). These tRFs might have resulted from decreased IRE1 $\alpha$  stringency in the sequence-specific cleavage of tRNA<sup>Gly(GCC)</sup> in vitro, or from tRNA<sup>Gly(GCC)</sup> structural alterations induced during purification or incubation. It is

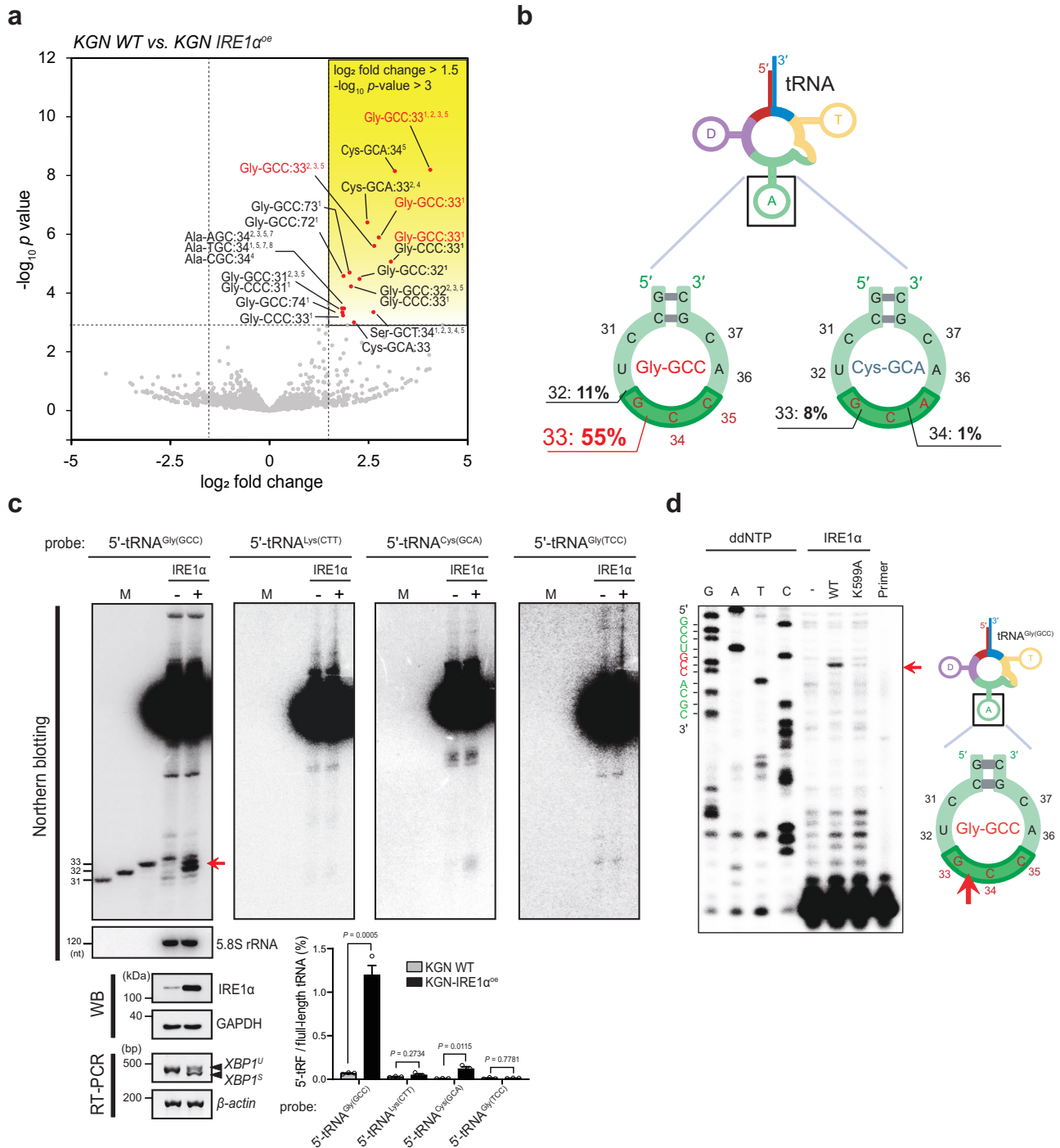


**Fig. 1 | Small RNA-seq analysis of IRE1 $\alpha$ -induced tRFs in vivo. a** Volcano plot depicting differentially expressed 5'-tRFs in WT and IRE1 $\alpha$ -overexpressing KGN cells (KGN-IRE1 $\alpha$ <sup>oe</sup>) ( $n = 3$ ). tRNA gene annotation: 'W-X:Y<sup>Z</sup>' (W: amino-acid; X: anticodon; Y: cleavage site; Z: unique gene identifier). Log<sub>2</sub> fold change >1.5 and  $p < 0.001$  was used as cut-off for significance (yellow box). **b** Based on the small RNA-seq analysis in **a**, cleavage sites at the anticodon loop in the secondary human tRNA<sup>Gly(GCC)</sup> and tRNA<sup>Cys(GCA)</sup> structures ( $n = 3$ ). Red: acceptor stem at 3'-end; Purple: D loop; light green: anticodon loop; dark green: anticodon; yellow: T loop; blue: CCA tail at 3'-end. Numbering in the anticodon indicates the 3'-end positions of the tRFs; percent indicates the proportion of 5'-tRFs in total 5'-tRFs (log<sub>2</sub> fold change >1.5 and  $p < 0.001$ ). **c** Northern blot analysis of tRNA fragments in KGN cells following IRE1 $\alpha$  overexpression KGN cells were transfected with plasmid encoding myc-tagged IRE1 $\alpha$  for 24 h, total RNA was extracted for analysis of 5'-tRNA

fragments by northern blotting. The expression of IRE1 $\alpha$  and GAPDH (loading control) was analysed by western blotting. Ribonucleolytic activity of IRE1 $\alpha$  was confirmed XBP1 splicing assay using RT-PCR analysis of unspliced/spliced (u/s) XBP1. Red arrow: 5'-tRFs from tRNA<sup>Gly(GCC)</sup> generated by IRE1 $\alpha$ . M: size marker. Percentage of 5'-tRF compared to full-length tRNA are shown. Data are presented as the mean  $\pm$  S.E.M ( $n = 3$ ).  $P$ -values were obtained by unpaired two-tailed  $t$ -test. **d** (Left) Primer extension analysis of 5'-end of tRNA<sup>Gly(GCC)</sup> fragment in KGN cells. KGN cells were transfected with a plasmid encoding IRE1 $\alpha$  or kinase defected mutant (IRE1 $\alpha$ -K599A). (Right) Secondary structure of mature tRNA<sup>Gly(GCC)</sup> and IRE1 $\alpha$  cleavage sites at anticodon. Numbering in the anticodon indicates the positions of mature tRNA nucleotides. Red arrow: prominent cleaved products of the tRNA<sup>Gly(GCC)</sup> generated by IRE1 $\alpha$ . Source data are provided as a Source Data file.

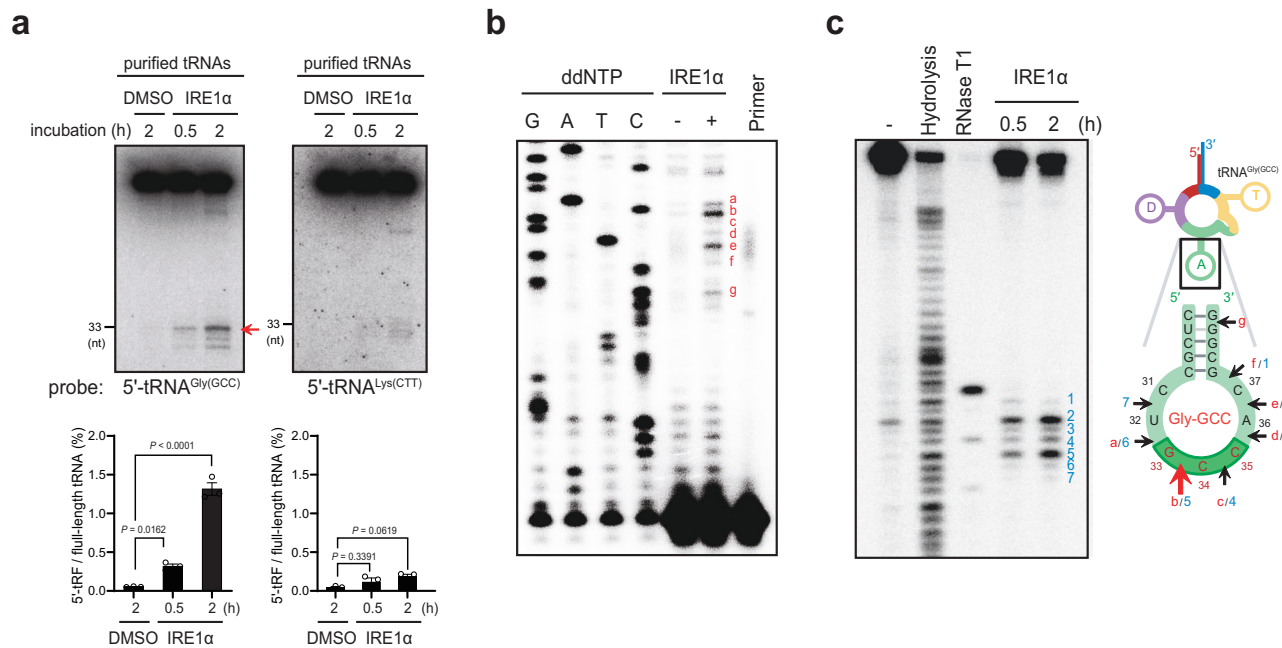


**Fig. 2 | IRE1 $\alpha$ -specific cleavage of tRNA<sup>Gly(GCC)</sup> in vitro.** **a** Northern blot analysis of in vitro cleaved tRNA<sup>Gly(GCC)</sup> and tRNA<sup>Lys(CTT)</sup> by recombinant IRE1 $\alpha$  (5 nM). Red arrow: prominent cleaved products of the tRNA<sup>Gly(GCC)</sup> generated by IRE1 $\alpha$ . The northern blot membranes were then stripped and reprobed with a <sup>32</sup>P-5'-end-labelled probe specific for the tRNA<sup>Lys(CTT)</sup>. Percentage of 5'-trf compared to full-length tRNA are shown. Values are presented as the mean  $\pm$  S.E.M ( $n = 3$ ).  $P$ -values were obtained by one-way ANOVA with Dunnett's multiple comparisons test. **b** Primer extension

assay on tRNA<sup>Gly(GCC)</sup> cleavage products in the presence of IRE1 $\alpha$  in vitro. IRE1 $\alpha$  cleavage sites in the tRNA<sup>Gly(GCC)</sup> are denoted by different letters (a–g). **c** In vitro cleavage of tRNA<sup>Gly(GCC)</sup> by IRE1 $\alpha$ . Purified tRNA<sup>Gly(GCC)</sup> (20 ng) was incubated with recombinant IRE1 $\alpha$  (5 nM) at 37 °C for 0.5 or 2 h. Secondary structure of mature tRNA<sup>Gly(GCC)</sup> and IRE1 $\alpha$  cleavage sites (a–g from Figs. 2b and 1–7 from Fig. 2c). Black arrows: position of the tRNA<sup>Gly(GCC)</sup> cleavage site generated by IRE1 $\alpha$ . Red arrow: major cleavage site by IRE1 $\alpha$ . Source data are provided as a Source Data file.

also possible that they arise from fragmentation of tRNA<sup>Gly(GCC)</sup> cleavage products.

These data clearly show the ability of IRE1 $\alpha$  to selectively cleave tRNA<sup>Gly(GCC)</sup> within the anticodon stem-loop. Furthermore, the cleavage site (C<sup>31</sup>UG  $\downarrow$  CCAC<sup>37</sup>) deduced from both small RNA-seq (Fig. 1a, b) and primer extension analyses of in vivo generated tRNA<sup>Gly(GCC)</sup> fragments (Fig. 1d) corresponded with the major in vitro IRE1 $\alpha$  cleavage product of tRNA<sup>Gly(GCC)</sup> (Fig. 2b, c). Based on these results, we designated 33-nt long 5'-trHs generated from the cleavage of tRNA<sup>Gly(GCC)</sup> at the overlapping site (C<sup>31</sup>UG  $\downarrow$  CCAC<sup>37</sup>) as 5'-trH-Gly<sup>GCC</sup>.

### Induction of 5'-trH-Gly<sup>GCC</sup> generation upon ER stress

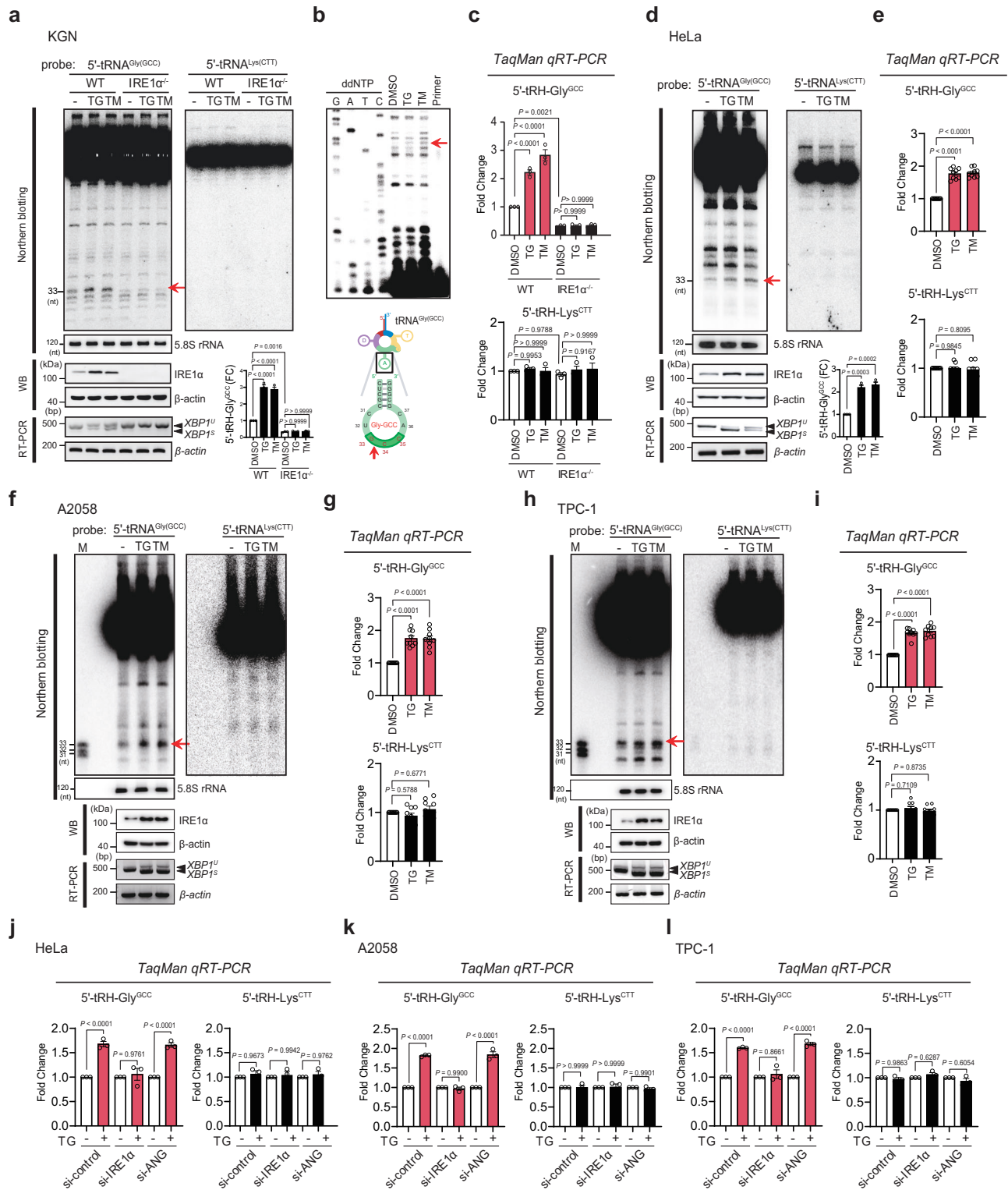
Considering that IRE1 $\alpha$  is an ER stress-activated endonuclease, we hypothesised that ER stress-induced activation of IRE1 $\alpha$  may cause generation of 5'-trH-Gly<sup>GCC</sup> from tRNA<sup>Gly(GCC)</sup> cleavage. To test this hypothesis, we induced ER stress in KGN cells using thapsigargin (TG) or tunicamycin (TM). Western blot analysis and an XBPI splicing assay confirmed that these agents stimulated the expression and ribonucleolytic activity of IRE1 $\alpha$  (Fig. 3a).

Next, ER stress-induced IRE1 $\alpha$  activation on tRNA cleavage was examined via northern blot analysis on tRNAs. In agreement with the effect of IRE1 $\alpha$  overexpression on the generation of trHs from tRNA<sup>Gly(GCC)</sup> (Fig. 1c), 5'-trH-Gly<sup>GCC</sup> levels were elevated approximately 3-fold while distinct trFs from other tRNAs were not detected following ER stress-induced IRE1 $\alpha$  expression (Fig. 3a and Supplementary Fig. 3a). This TG- or TM-induced production of 5'-trHs was not observed in IRE1 $\alpha$  knockout cells (IRE1 $\alpha$ <sup>-/-</sup>; Fig. 3a and Supplementary Figs. 3b, 4a–c). In addition, we found that the cleavage pattern of these 5'-trHs resembled those generated by IRE1 $\alpha$ , which cleaves tRNA<sup>Gly(GCC)</sup> between positions 33 and 34 within the anticodon stem-loop (C<sup>31</sup>UG  $\downarrow$  CCAC<sup>37</sup>) (Fig. 3b). We obtained analogous results from TaqMan-based real-time PCR using 33-mer 5'-trH-Gly<sup>GCC</sup> specific primers (Fig. 3c and Supplementary Fig. 3c, d); 5'-trH-Gly<sup>GCC</sup> levels were

elevated 2.2 or 2.5-folds in WT KGN cells following TG or TM treatment, respectively, whereas they were not significantly changed in IRE1 $\alpha$ <sup>-/-</sup> cells upon ER-stress (Fig. 3c). Hence, ER stress-induced 5'-trH-Gly<sup>GCC</sup> production is mediated by IRE1 $\alpha$ -dependent tRNA<sup>Gly(GCC)</sup> cleavage in KGN cells.

We further investigated whether angiogenin (ANG) is involved in 5'-trH-Gly<sup>GCC</sup> production upon ER stress since this ribonuclease is known to produce trHs by cleaving the anticodon loop region of tRNAs in stress response<sup>4,5</sup>. First, ANG overexpression resulted in high levels of 5'-trFs from all tRNA species tested (tRNA<sup>Gly(GCC)</sup>, tRNA<sup>Lys(CTT)</sup>, and tRNA<sup>Val(TAC)</sup>; Supplementary Fig. 3e), indicating that selective production of 5'-trH-Gly<sup>GCC</sup> upon ER stress is not likely mediated by ANG. In addition, we observed that alterations in IRE1 $\alpha$  expression levels by knockout of the *IRE1 $\alpha$*  gene, exogenous overexpression, or ER stress did not significantly affect ANG expression (Supplementary Fig. 3f, g). These results indicate that 5'-trH-Gly<sup>GCC</sup> production is directly related to IRE1 $\alpha$  expression, not to regulation of ANG expression by IRE1 $\alpha$ . Furthermore, northern blot analysis showed a 2.7-fold increase in the abundance of 5'-trH-Gly<sup>GCC</sup> fragments in samples taken from both WT and ANG knockout KGN (ANG<sup>-/-</sup>) cells when treated with TG compared to those from DMSO-treated cells (Supplementary Figs. 3h and 4d–f). We obtained analogous results from TaqMan assays (Supplementary Fig. 3i). Together, these results demonstrated that ANG is not involved in ER stress-induced 5'-trH-Gly<sup>GCC</sup> production in KGN cells.

To investigate whether the production of 5'-trHs from tRNA<sup>Gly(GCC)</sup> is commonly coupled with ER stress in other human cancer cells, we induced ER stress in HeLa, A2058 melanoma, and papillary thyroid cancer (TPC-1) cells with TG or TM and analysed 5'-trHs production. ER stress-dependent selective generation of 5'-trHs from tRNA<sup>Gly(GCC)</sup> was also observed in these cancer cells (Fig. 3d–i). Once again, ER stress-induced 5'-trH-Gly<sup>GCC</sup> production is positively correlated with IRE1 $\alpha$  expression and is independent of ANG expression in these cancer cells (Fig. 3j–l).



### Proteins bound with 5'-tRH-Gly<sup>GCC</sup>

To investigate the functional role of 5'-tRH-Gly<sup>GCC</sup>, we characterised proteins bound to 5'-tRH-Gly<sup>GCC</sup> in KGN cells via biotinylation of the tRH 5'- and 3'-ends. Specifically, 33-nt long 5'-tRHs of tRNA<sup>Gly(GCC)</sup> (5'-tRH-Gly<sup>GCC</sup> mimic) were used. To assess non-specific protein binding of biotinylated RNA with a streptavidin coated microplate, 5'-biotin-oligo A8 RNA and 3'-biotin- tRH-Gly<sup>GCC</sup> were used as controls. Two protein bands near 70 kDa and 55 kDa appeared to specifically bind to a 5'-biotin-tRH-Gly<sup>GCC</sup> in both samples of TG-treated and -untreated cells but did not bind 3'-biotin- tRH-Gly<sup>GCC</sup> or 5'-biotin-oligo A8 RNA

(Supplementary Fig. 5a, right panel). The comparative tandem mass spectrometry analysis of proteins interacting with biotinylated RNA showed that the heterogeneous nuclear ribonucleoprotein M isoform b (HNRNPM) and heterogeneous nuclear ribonucleoprotein H (HNRNPH2) in TG-treated and -untreated samples were enriched at similar levels in the microplate containing 5'-biotin-tRH-Gly<sup>GCC</sup> (Supplementary Fig. 5b and Supplementary Table 2). These nuclear proteins may be potential binding partners of the 5'-tRHs of tRNA<sup>Gly(GCC)</sup>. We were also able to detect a moderate amount of HNRNPF, while HNRNPH1 was not detected. Orthologues of HNRNP proteins have

**Fig. 3 | ER stress induces 5'-tRHs cleavage by tRNA<sup>Gly(GCC)</sup>.** **a** Northern blot analysis of tRNA<sup>Gly(GCC)</sup> fragments in control KGN (WT) or IRE1 $\alpha$  knockout-KGN cells (IRE1 $\alpha$ <sup>-/-</sup>) ( $n = 3$ ). Cells were treated with 0.1% DMSO, TG (0.1  $\mu$ M) or TM (1  $\mu$ g/ml) for 6 h and harvested. Total RNA was isolated and probed with a probe specific for the tRNA<sup>Gly(GCC)</sup>. The northern blot membranes were then stripped and reprobed with a <sup>32</sup>P-5'-end-labelled probe specific for the tRNA<sup>Lys(CTT)</sup>. Quantification of 5'-tRH-Gly<sup>GCC</sup> level is presented in the bottom panel. **b** (Upper) 5'-end of tRNA<sup>Gly(GCC)</sup> fragment detected in **a** (KGN WT) determined by primer extension analysis. (Lower) Secondary structure of mature tRNA<sup>Gly(GCC)</sup> and IRE1 $\alpha$  cleavage sites at anticodon stem loop. Red arrow: major IRE1 $\alpha$  cleavage site. **c** Validation of 5'-tRH enrichment following treatment of KGN WT and IRE1 $\alpha$ <sup>-/-</sup> cells with 0.1  $\mu$ M of TG by TaqMan-based real-time PCR. Data are presented as the mean  $\pm$  S.E.M ( $n = 3$ ). Northern blot analysis of tRNA<sup>Gly(GCC)</sup> fragments in HeLa (**d**), A2058 (**f**), and TPC-1 (**h**) cells ( $n = 3$ ). Total RNA

was isolated and probed with a probe specific for the tRNA<sup>Gly(GCC)</sup>. The northern blot membranes were then stripped and reprobed with a <sup>32</sup>P-5'-end-labelled probe specific for the tRNA<sup>Lys(CTT)</sup>. Quantification of 5'-tRH-Gly<sup>GCC</sup> level presented in the bottom panel of **d**. Validation of 5'-tRH enrichment following treatment of HeLa (**e**), A2058 (**g**), and TPC-1 (**i**) cells with DMSO, TG or TM by TaqMan-based real-time PCR ( $n = 9$ ). TaqMan-based real-time PCR of tRNA<sup>Gly(GCC)</sup> or tRNA<sup>Lys(CTT)</sup> fragments in IRE1 $\alpha$  knockdown or ANG knockdown HeLa (**j**), A2058 (**k**), and TPC-1 (**l**) cells with TG (0.1  $\mu$ M), respectively. In **a**, **d**, **f**, and **h**, the expression of IRE1 $\alpha$  and  $\beta$ -actin (loading control) was analysed by western blotting (WB). Ribonucleolytic activity of IRE1 $\alpha$  was confirmed XBPI splicing assay using RT-PCR analysis of unspliced/spliced (u/s) XBPI. *P*-values were obtained by one-way ANOVA with Turkey's multiple comparisons. Red arrow: tRHs cleaved by IRE1 $\alpha$ . Source data are provided as a Source Data file.

been previously identified as binding proteins of tRH<sup>Gly(GCC)</sup> in mouse cells<sup>31</sup>.

We assessed the physical interaction between 5'-tRH-Gly<sup>GCC</sup> and HNRNP proteins via electrophoretic mobility shift assay (EMSA) using purified HNRNPM and HNRNPH2 recombinant proteins and 5'-<sup>32</sup>P-labelled synthetic 5'-tRH-Gly<sup>GCC</sup> and 5'-tRH-Lys<sup>CTT</sup>. These proteins bind 5'-tRH-Gly<sup>GCC</sup> with much higher affinity than 5'-tRH-Lys<sup>CTT</sup> (Supplementary Fig. 6a), providing evidence of specific interactions between 5'-tRH-Gly<sup>GCC</sup> and HNRNP proteins.

We further tested physical interaction of 5'-tRH-Gly<sup>GCC</sup> or 3'-tRH-Gly<sup>GCC</sup> with HNRNP proteins (HNRNPM and HNRNPH2) by using the surface plasmon resonance (SPR). In SPR assay, both 5'-tRH-Gly<sup>GCC</sup> and scramble RNA showed dose-dependent binding signal to the immobilized HNRNPM and HNRNPH2 (Supplementary Fig. 6b). However, kinetic analysis indicated that 5'-tRH-Gly<sup>GCC</sup> has about 10–35 times higher affinities for HNRNPM and HNRNPH2 with  $K_D$  of 86.30 nM and 27.07 nM, compared to 3'-tRH-Gly<sup>GCC</sup>, which showed affinities for HNRNPM and HNRNPH2 with  $K_D$  of 959 nM and 938 nM, respectively (Supplementary Fig. 6c). These results provide clear evidence for specific and strong interaction between 5'-tRH-Gly<sup>GCC</sup> and HNRNP proteins.

We further investigated tRF species that bind to these HNRNP species by performing RNA immunoprecipitation followed by next-generation sequencing (RIP-seq) using tagged HNRNPH2 (Flag-HNRNPH2) or HNRNPM (HA-HNRNPM) proteins (Fig. 4a). In our RIP-seq data, while the average proportion of tRNA-derived reads in the total reads was 20.2% in the input, it was 0.36% and 3.24% in HNRNPM and HNRNPH2 immunoprecipitates, respectively (Fig. 4b). Notably, the HNRNPM and HNRNPH2 immunoprecipitates showed 37.7- and 17.3-fold enrichment of rRNA-derived reads, respectively, compared to the input. The proportions of genes mapped to other regions of the genome, including mRNAs, pseudogenes, and non-coding genes, were not significantly different between the input and HNRNP immunoprecipitates.

As shown in Fig. 4c, tRFs-Gly<sup>GCC</sup> was the most abundantly enriched tRF in the HNRNPM- and HNRNPH2 immunoprecipitates, comprising 89.7% and 36.8% of the total, respectively. The 5'-tRH-Gly<sup>GCC</sup> (3'-end corresponding to position 33 of tRNA<sup>Gly(GCC)</sup>) was the only tRH-Gly<sup>GCC</sup> predominantly recruited with both HNRNPM and HNRNPH2 in comparison to the input control (Fig. 4d). In sharp contrast, tRNA<sup>Lys(GCA)</sup> the other highly detected tRF following IRE1 $\alpha$  overexpression (Fig. 1a, b) was not found to be enriched in either HNRNPM or HNRNPH2 RIP-seq samples (Fig. 4e), supporting the specific association of 5'-tRH-Gly<sup>GCC</sup> with HNRNP proteins. We also obtained analogous results from TaqMan-based real-time PCR using 33-mer 5'-tRH-Gly<sup>GCC</sup>-specific primers (Fig. 4f). In addition, results from these molecular analyses including RIP-seq and real-time PCR are in accordance with the results obtained from our biochemical analyses where HNRNPH2 exhibits higher binding affinity to 5'-tRH-Gly<sup>GCC</sup> than HNRNPM (Supplementary Fig. 6a–c). Thus, together, these results provide clear evidence for a specific and robust interaction between the 33-mer 5'-tRH-Gly<sup>GCC</sup> and HNRNP proteins in vivo. We additionally conducted RNA pull-down

assays to detect the interactions between IRE1 $\alpha$ , HNRNPM, or HNRNPH2 to 5'-tRH-Gly<sup>GCC</sup>. As anticipated, precipitation of biotin-labelled 5'-tRH-Gly<sup>GCC</sup> probes led to the enrichment of HNRNPM and HNRNPH2 compared to that of biotin-labelled control probes. Enrichment of IRE1 $\alpha$  was not observed, suggesting that IRE1 $\alpha$  is released from tRNA fragments subsequent to the cleavage of mature tRNAs (Fig. 4g). These results cohesively validate our results in Supplementary Figs. 5 and 6.

### Roles of ER stress-induced 5'-tRH-Gly<sup>GCC</sup>

To investigate functional roles for 5'-tRH-Gly<sup>GCC</sup> in cancer cells that produced these 5'-tRHs upon ER stress, KGN, HeLa, and A2058 cells were treated with synthetic 5'-tRH-Gly<sup>GCC</sup> (5'-tRH-Gly<sup>GCC</sup> mimic) and two other control tRH mimics (scramble and 5'-tRH-Lys<sup>CTT</sup>). Treatment with 5'-tRH-Gly<sup>GCC</sup> mimic increases viable cell number in a manner dependent on mimic concentrations, which increased cell number of KGN, HeLa, and A2058 by 34%, 25%, and 27%, respectively, at the highest concentration of the mimic used (Fig. 5a–c). The controls did not significantly affect cell viability (Fig. 5a–c).

Blocking the 5'-tRH-Gly<sup>GCC</sup> mimics with complementary antisense DNA oligos (ASOs; anti-5'-tRH) abolished the positive effects of 5'-tRH-Gly<sup>GCC</sup> on viability of KGN cells (Supplementary Fig. 7a). We validated that these ASOs bind selectively to tRHs over full-length tRNAs (Supplementary Fig. 7b, c). The enhancement of cell viability by 5'-tRH-Gly<sup>GCC</sup> mimic occurred due to increased proliferation of KGN cells (Supplementary Fig. 7d), as no effect on apoptosis was observed (Supplementary Fig. 7e). In addition, tRH mimic did not affect the migration capability of KGN cells (Supplementary Fig. 7f). Taken together, these results suggest that 5'-tRH-Gly<sup>GCC</sup> functions to control cancer cell proliferation.

Next, we investigated whether HNRNPM and HNRNPH2 participate in 5'-tRH-Gly<sup>GCC</sup>-mediated cell proliferation. The 5'-tRH-Gly<sup>GCC</sup> mimic-induced promotion of cell viability in KGN and HeLa cells was abolished following HNRNPM or HNRNPH2 knockdown (Fig. 5d, e, Supplementary Fig. 7g, h). Transfection of the 5'-tRH-Gly<sup>GCC</sup> mimics in HNRNPM or HNRNPH2-depleted KGN (Fig. 5d) or HeLa (Fig. 5e) cells further reduced cell survival compared to those treated with control mimics at different degrees, suggesting that HNRNPM and HNRNPH2 might have a cell line-specific role in 5'-tRH-Gly<sup>GCC</sup>-mediated cell survival. Hence, 5'-tRH-Gly<sup>GCC</sup>-mediated promotion of cell proliferation depends on its interaction with HNRNP proteins in these cancer cells. Considering analogous results obtained following the knockdown of HNRNPF/H1/H2 (Supplementary Fig. 7i, j), we think that the 5'-tRH-Gly<sup>GCC</sup> might interact with multiple nuclear ribonucleoproteins for cellular function.

We further examined whether IRE1 $\alpha$ -dependent 5'-tRH-Gly<sup>GCC</sup> generation mediates the ER stress-induced effect on cell viability. Treatment with ASOs targeting endogenous 5'-tRH-Gly<sup>GCC</sup> (anti-5'-tRH-Gly<sup>GCC</sup>) significantly potentiated TG-induced cell death in WT KGN cells compared to those treated with anti-5'-tRH-Lys<sup>CTT</sup> (Fig. 5f). In contrast, anti-5'-tRH-Gly<sup>GCC</sup> did not elicit such an effect in IRE1 $\alpha$ <sup>-/-</sup> cells (Fig. 5f).

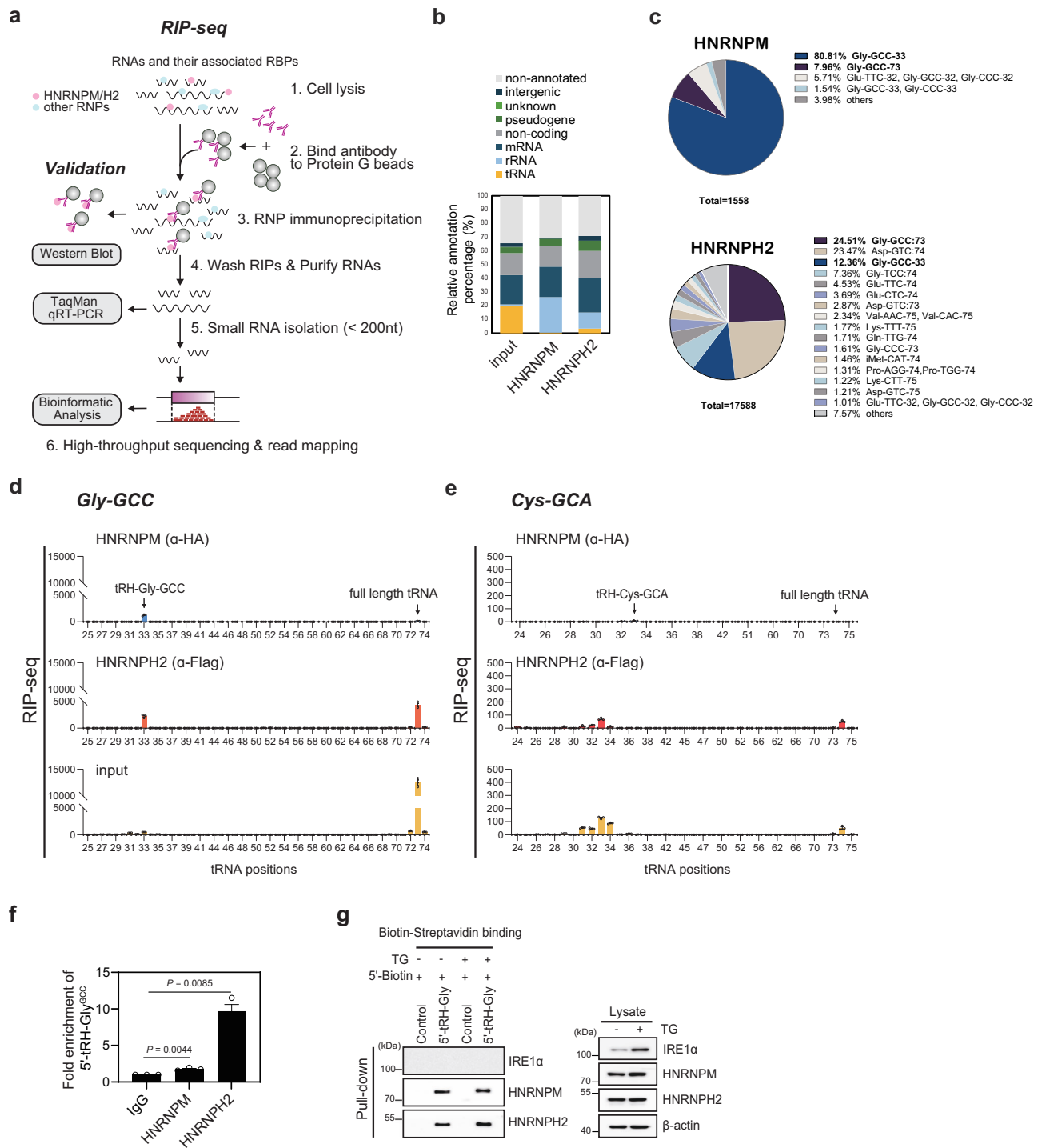


**Fig. 4 | Confirmation of specific association of HNRNPM and HNRNPH2 with 5'-tRH-Gly<sup>GCC</sup> by RIP-seq analysis.** **a** Experimental design scheme for RIP-seq analysis. A2058 cells were transfected with expression vectors encoding indicated proteins (myc-IRE1 $\alpha$ , HA-HNRNPM, FLAG-HNRNPH2), and cell extracts were prepared and immunoprecipitated with anti-HA or anti-FLAG antibodies. Three independent experiments were performed. **b** The proportion of RIP-seq enriched RNA fragments annotated to the indicated RNAs ( $n = 3$ ). **c** Percentage of enriched tRF with HNRNPH2 (upper) or HNRNPM (lower) ( $n = 3$ ). The pie chart represents the proportion of tRFs in each of the total tRF read counts in RIP-seq data. Mapped read counts from RIP-seq of tRF-Gly<sup>GCC</sup> (**d**) or tRF-Cys<sup>GCA</sup> (**e**) associated with HNRNPH2 (red) and HNRNPM (blue) were normalised to the corresponding read counts from

the input. Data are presented as the mean  $\pm$  S.E.M ( $n = 3$ ). **f** Quantification of 5'-tRH-Gly<sup>GCC</sup> enriched with HNRNPM or HNRNPH2 proteins. Co-immunoprecipitated RNAs from the indicated antibodies in A2058 cells were analysed by TaqMan-based qRT-PCR using designed probes on the 33-mer 5'-tRH-Gly<sup>GCC</sup>. Data are presented as the mean  $\pm$  S.E.M ( $n = 3$ ).  $P$ -values were obtained by One sample  $t$ -test. **g** Pull-down of HNRNPM and HNRNPH2 using 5'-biotinylated tRH-Gly<sup>GCC</sup>. TG (0.1  $\mu$ M)-treated (+) or -untreated (-) KGN cell lysates were combined with 5'-biotinylated tRH-Gly<sup>GCC</sup> or 5'-biotin-oligo A8 RNA (control). After allowing the binding of protein and RNA, streptavidin-coated beads were used to pull down the RNA. After washing, RNA-bound IRE1 $\alpha$ , HNRNPM, or HNRNPH2 proteins were visualised using western blot. Source data are provided as a Source Data file.

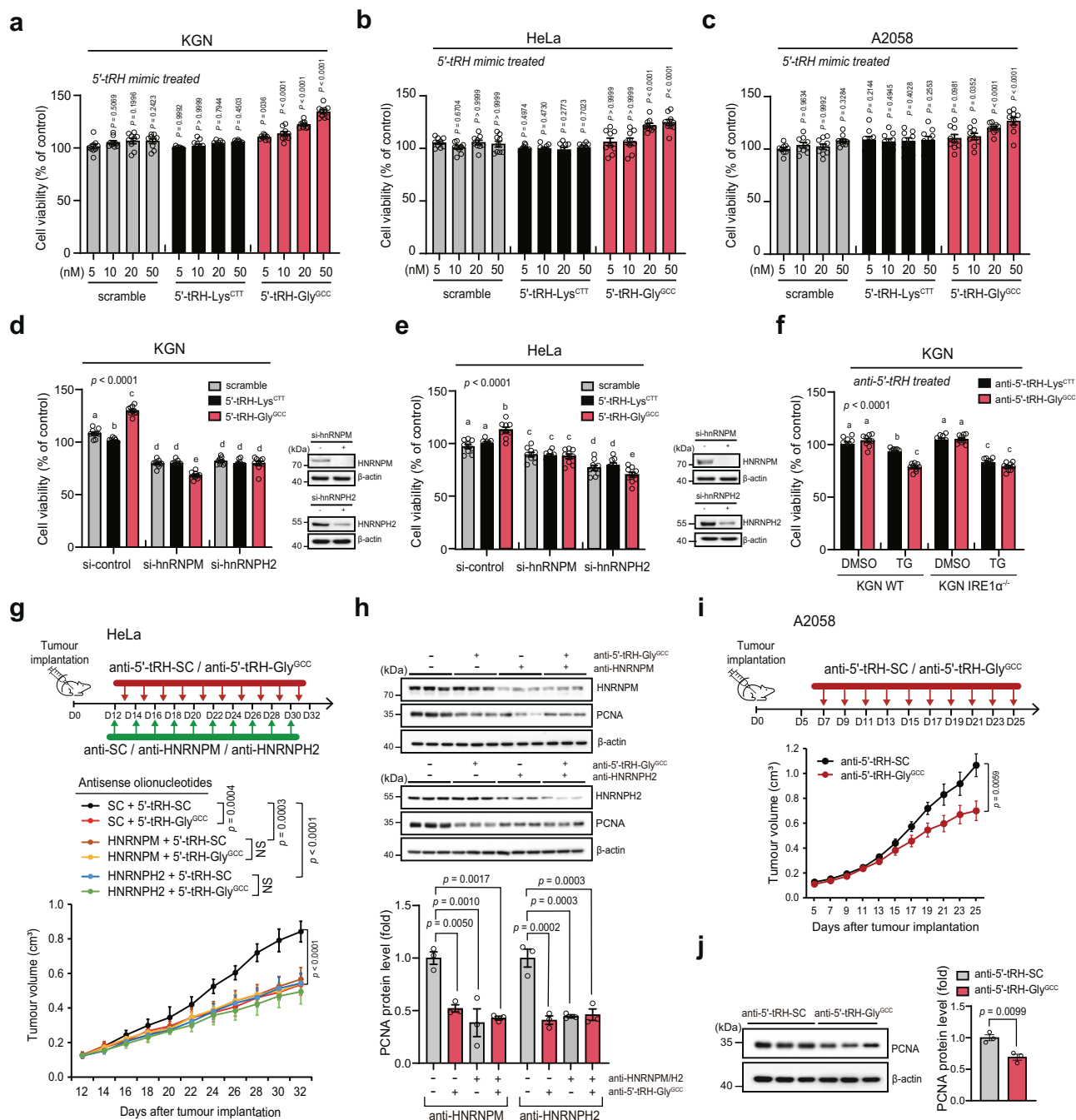


**Fig. 5 | Functional roles of 5'-tRFs of tRNA<sup>Gly(GCC)</sup>.** Cell viability of KGN (a), HeLa (b), and A2058 (c) cells following transfection with increasing amounts of tRH mimics. Data are presented as the mean ± S.E.M ( $n = 9$ ).  $P$ -values were obtained by one-way ANOVA with Dunnett's multiple comparisons test. Cell viability of KGN (d) and HeLa (e) cells following transfection with siRNAs for HNRNPM or HNRNPH2 and tRH mimics (left). Knockdown efficiency of HNRNPM or HNRNPH2 proteins was determined (right). The expression of HNRNPM or HNRNPH2, and β-actin (loading control) was analysed by western blotting. Data are presented as the mean ± S.E.M ( $n = 9$ ). f Cell viability of WT and IRE1α<sup>-/-</sup> KGN cells following transfection with ASOs targeting endogenous 5'-tRHs (anti-5'-tRH-Lys<sup>CTT</sup> or anti-5'-tRH-Gly<sup>GCC</sup>) in the absence or presence of TG. Data are presented as the mean ± S.E.M ( $n = 9$ ). In e–f, different letters denote statistically significant differences ( $p < 0.0001$ ; two-way ANOVA with Student–Newman–Keuls multiple comparisons test). g–j Antitumor effects of anti-5'-tRH-Gly<sup>GCC</sup> in HeLa cell- or A2058 cell-derived mice xenograft tumour model. g After HeLa cell-derived subcutaneous xenograft

reached about 100 mm<sup>3</sup>, mice ( $n = 10$  per each group) were treated with AuNP<sup>DT</sup> loaded with anti-scramble, anti-HNRNPM, or anti-HNRNPH2, followed by alternate injections of AuNP<sup>DT</sup> loaded with anti-scramble or anti-5'-tRH-Gly<sup>GCC</sup> every other day.  $P$ -values were obtained by two-way ANOVA with Dunnett's multiple comparisons test. h Representative immunoblots and quantified data for tumours from each group are presented. Data are presented as the mean ± S.E.M ( $n = 3$ ).  $P$ -values were obtained by one-way ANOVA with Dunnett's multiple comparisons test. i Volumes of A2058 cell-derived subcutaneous xenograft tumours from mice injected with either the AuNP<sup>DT</sup>-anti-scramble as a control, or AuNP<sup>DT</sup>-anti-5'-tRH-Gly<sup>GCC</sup> were measured ( $n = 12$  per each group).  $P$ -values were obtained by unpaired two-tailed  $t$ -test. j Representative immunoblots and quantified data for tumours from each group are presented. Data are presented as the mean ± S.E.M ( $n = 3$ ).  $P$ -values were obtained by unpaired two-tailed  $t$ -test. The images of the mouse model were generated from the stock images of PowerPoint. Source data are provided as a Source Data file.



Thus, these data imply that IRE1 $\alpha$  cleavage-generated 5'-tRH-Gly<sup>GCC</sup> contributes to cellular adaptation upon ER stress.

To investigate *in vivo* 5'-tRH-Gly<sup>GCC</sup> function, we silenced the endogenous 5'-tRH-Gly<sup>GCC</sup> or HNRNPM/H2 by delivering ASOs against them using a functionalized gold nanoparticle (AuNP)-based delivery system (AuNP<sup>dt</sup>)<sup>32</sup> in a xenograft mouse model. First, we investigated the relevance of HNRNPs for tumour growth in xenograft models by injecting ASOs specific to HNRNPM or HNRNPH2 into HeLa cell-xenografted tumours. As shown in Fig. 5g, tumour growth in mice treated with AuNP<sup>dt</sup> loaded with anti-5'-tRH-Gly<sup>GCC</sup> was prominently inhibited compared with that treated with AuNP<sup>dt</sup> loaded with scramble (Fig. 5g). In addition, following depletion of HNRNPM or HNRNPH2, the anti-5'-tRH-Gly<sup>GCC</sup> treatment did not further inhibit tumour growth in mice (Fig. 5g), indicating that the anti-tumour function of 5'-tRH-Gly<sup>GCC</sup> requires expression of HNRNPM and HNRNPH2. Consistent with anti-proliferative response observed in HeLa cancer cells treated with anti-5'-tRH-Gly<sup>GCC</sup> *in vitro* (Supplementary Fig. 7k), proliferating cell nuclear antigen (PCNA) expression in tumours decreased by ~44% upon anti-5'-tRH-Gly<sup>GCC</sup> treatment in xenografted tumours (Fig. 5h).

To investigate whether the phenomenon of anti-5'-tRH-Gly<sup>GCC</sup>-induced inhibition of tumour growth is generally observed in different cancer types, we conducted similar experiments using the A2058 melanoma cell line. Likewise, A2058 cell-derived xenograft tumour growth in mice treated with AuNP<sup>dt</sup> loaded with anti-5'-tRH-Gly<sup>GCC</sup> was prominently inhibited compared with that treated with scramble DNA (Fig. 5i). Similarly, consistent with anti-proliferative response observed in A2058 cancer cells treated with anti-5'-tRH-Gly<sup>GCC</sup> *in vitro* (Supplementary Fig. 7l), PCNA expression in tumours decreased by ~31% upon anti-5'-tRH-Gly<sup>GCC</sup> treatment in xenografted tumours (Fig. 5j). During the whole experiment, no significant weight loss or any other obvious signs of toxicity were observed in any of the AuNP<sup>dt</sup> loaded with ASOs-treated mice (Supplementary Fig. 7m, n).

### Effect of 5'-tRH-Gly<sup>GCC</sup> in alternative splicing

To dissect the relevance of 5'-tRH-Gly<sup>GCC</sup> functioning, we performed total transcriptome analysis on KGN cells transfected with 5'-tRH-mimics. The RNA abundance of 66 genes was altered more than 1.5-fold in cells transfected with 5'-tRH-Gly<sup>GCC</sup> mimics compared to those with 5'-tRH-Lys<sup>CTT</sup> mimics (Fig. 6a and Supplementary Table 3). Functional annotation analysis further indicated that most genes were enriched in alternative splicing and phosphoproteins (Fig. 6b and Supplementary Table 4). Based on these results, and the fact that 5'-tRH-Gly<sup>GCC</sup> interacts with multiple nuclear proteins functioning in RNA splicing. For this reason, we further analysed isoforms of total transcripts using nanopore sequencing and FLAIR (full-length alternative isoform analysis of RNA) modules<sup>33</sup>.

We analysed four main types of alternative splicing events (alternative 3'- and 5'-splicing, intron retention, and exon skipping events) associated with isoform formation. Compared to the control group (5'-tRH-Lys<sup>CTT</sup>), we identified 19 differential isoforms from the 17 genes in the 5'-tRH-Gly<sup>GCC</sup>-treated group, where one or more of their junctions exhibited alternative 5'/3' splice site selection or exon skipping (Supplementary Table 5). These genes had multiple alternative splicing events within their transcripts, except *CFDPI* (exon skipping), *PRDX4* (alternative 5'-splicing), and *MAGED2* (alternative 3'-splicing) (Supplementary Table 5). Among them, the isoform usage of *ELOB* (Fig. 6c, upper panel) and *PSMB5* (Fig. 6c, lower panel) was significantly altered between 5'-tRH-Lys<sup>CTT</sup>- and 5'-tRH-Gly<sup>GCC</sup>-treated groups.

In addition, to validate the alternative splicing patterns observed in response to 5'-tRH-Gly<sup>GCC</sup> levels, we conducted RT-PCR using common primer pairs that could simultaneously amplify different splicing variants within a single reaction. As shown in Fig. 6d, a 5'-tRH-Gly<sup>GCC</sup> mimic induced mRNA levels of a truncated variant (isoform 4 of *ELOB* and isoform 1 of *PSMB5*), whereas it decreased mRNA levels of longer

variants (isoform 3 of *ELOB* and isoform 4 of *PSMB5*). However, the knockdown of *HNRNPH2* or *HNRNPM* abolished these effects of 5'-tRH-Gly<sup>GCC</sup> on the alterations of isoform profiles. These results indicate that 5'-tRH-Gly<sup>GCC</sup>-mediated alterations in mRNA isoform biogenesis of these genes is dependent on HNRNPH2 and HNRNPM (Fig. 6d).

We observed that an ER stress-inducing agent, TM, had a similar effect on the splice variant composition of *ELOB* and *PSMB5* genes as by 5'-tRH-Gly<sup>GCC</sup> mimics shown in Fig. 6e (Fig. 6f). In contrast, these effects were absent in IRE1 $\alpha$  knockout-KGN (IRE1 $\alpha$ <sup>-/-</sup>) cells (Fig. 6f), indicating that ER stress-induced alterations in alternative splicing of these mRNAs are dependent on IRE1 $\alpha$  activity. Sequestering of 5'-tRH-Gly<sup>GCC</sup> by ASOs in xenografted tumours resulted in a reverse effect on mRNA isoform composition (Fig. 6g, h) observed in cancer cells treated with 5'-tRH-Gly<sup>GCC</sup> mimics or TG in Fig. 6e, f. Treatment of tumours with anti 5'-tRH-Lys<sup>CTT</sup> did not affect isoform composition of these genes (Fig. 6g, h).

Hence, 5'-tRH-Gly<sup>GCC</sup> levels affect alternative splicing events, leading to alterations in the transcript isoform profile.

### Nucleus localisation of tRH-Gly<sup>GCC</sup>

Our results showing an interaction between tRH-Gly<sup>GCC</sup> and nuclear proteins (Supplementary Fig. 5), as well as the effect of tRH-Gly<sup>GCC</sup> mimics on transcript isoform profiles (Fig. 6), suggest that tRH-Gly<sup>GCC</sup> functions within the nucleus. Thus, to determine the subcellular distribution of ER stress-induced 5'-tRHs of tRNA<sup>Gly(GCC)</sup>, we conducted a fluorescent *in situ* hybridisation assay (FISH), with a probe designed to recognise 5'-tRHs of tRNA<sup>Gly(GCC)</sup>. This assay was performed under conditions designed to avoid the denaturation of stable mature tRNAs and hybridisation of the probe to full-length tRNAs. Fluorescent signals, obtained with the probe recognising the 5'-tRHs of tRNA<sup>Gly(GCC)</sup>, displayed a nucleus-associated localisation pattern with higher signal intensity following TG-induced ER stress, compared to treatment with dimethylsulphoxide (DMSO; Supplementary Fig. 8a). To confirm the specificity of the hybridisation probe, we performed a series of experiments under non-denaturing or denaturing conditions using an additional control probe. This control probe (anticodon bridging probe) bridged the 5'- and 3'-regions spanning the nucleotides that encompass the anticodon and was designed to detect only intact full-length tRNAs with minimal complementarity for 5'-tRHs of tRNA<sup>Gly(GCC)</sup>. The anticodon bridging probe showed a fluorescent signal under denaturing FISH conditions, while no signal was observed under non-denaturing conditions (Supplementary Fig. 8a). Hence, 5'-tRHs of tRNA<sup>Gly(GCC)</sup> were definitively recognised with the specific probe used under our experimental conditions. In addition, measurement of tRH-Gly<sup>GCC</sup> distribution by TaqMan assay and Northern blot analysis showed that 33 nt-long 5'-tRH-Gly<sup>GCC</sup> levels were specifically elevated approximately 1.7- and 4.6-fold, respectively, in the nuclear fraction of KGN cells following TG treatment over the 6 h period (Supplementary Fig. 8b, c). These results indicate that 33 nt-long 5'-tRHs of tRNA<sup>Gly(GCC)</sup> localise to the nucleus when cells are subjected to ER stress.

### IRE1 $\alpha$ -dependent 5'-tRH<sup>Gly(GCC)</sup> cleavage in other organisms

To investigate whether IRE1 $\alpha$ -mediated generation of 5'-tRH-Gly<sup>GCC</sup> upon ER stress occurs in other eukaryotic species, we analysed selective generation of 5'-tRH-Gly<sup>GCC</sup> in an acute ER stress murine model<sup>34</sup> and ER-stressed yeast species, *Cryptococcus neoformans*. IRE1 homologues of mouse and yeast show 94.40% and 40.15% sequence similarity, respectively to the protein kinase and kinase-extension nuclease domains of human IRE1 $\alpha$ .

We observed prominent induction of IRE1 $\alpha$  expression in the ovary, liver, epididymis, kidney, and pancreas of ER-stressed mice (Supplementary Fig. 9a). Northern blot analysis showed an increased abundance of 5'-tRH-Gly<sup>GCC</sup> fragments in the ovary (Fig. 7a), liver (Supplementary Fig. 9b), and epididymis (Supplementary Fig. 9c) in samples taken from ER-stressed mice compared to control mice samples, while other tRNA

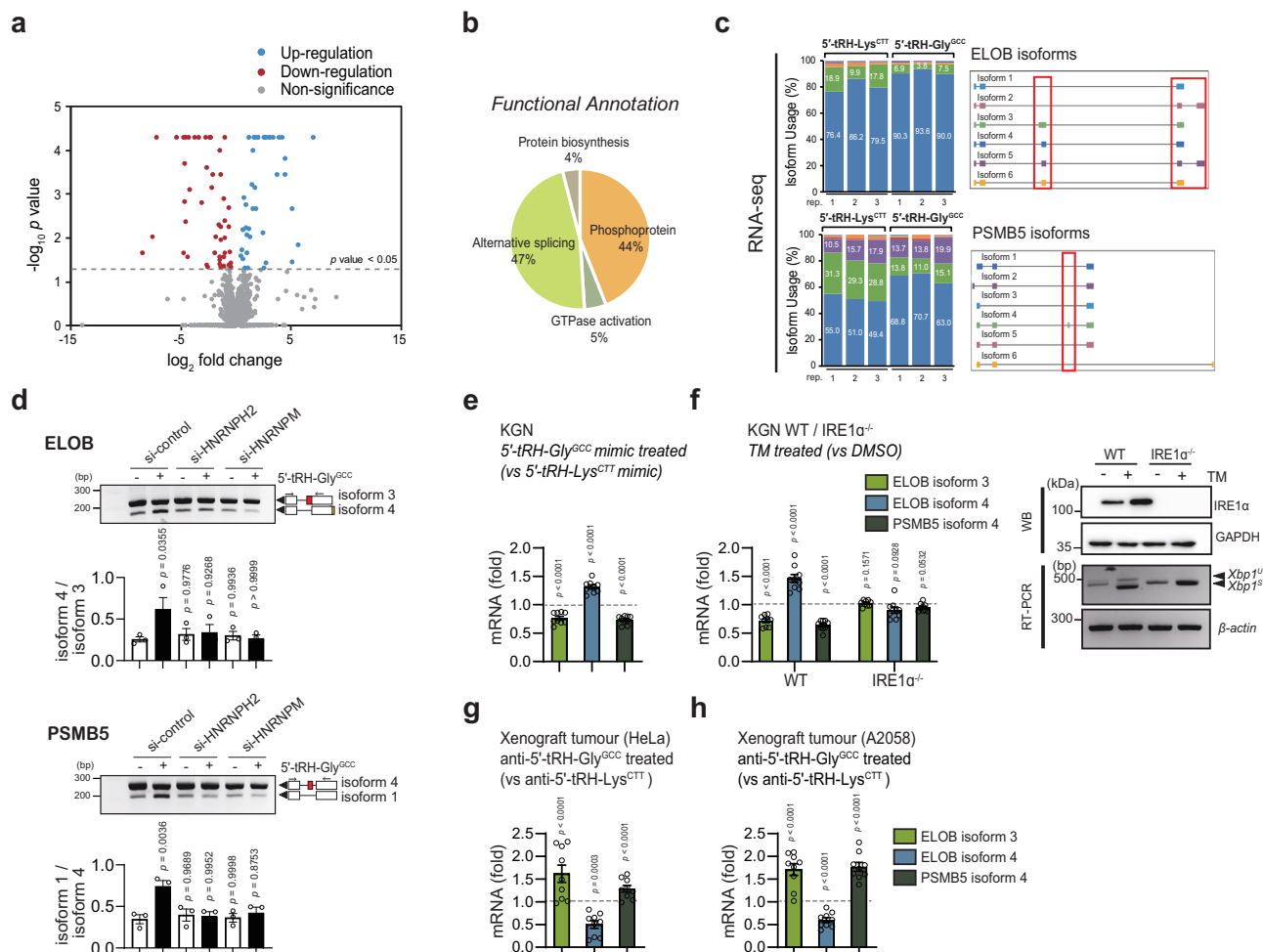


**Fig. 6** | 5'-tRH-Gly<sup>GCC</sup> mediates alternative splicing events. **a** Volcano plot of differentially expressed protein-coding genes in KGN cells transfected with 5'-tRH-Gly<sup>GCC</sup> mimic and control KGN cells transfected with 5'-tRH-Lys<sup>CTT</sup> mimic ( $n = 2$ ). Blue dots: significant upregulation of target genes; red dots: significant down-regulation of target genes. **b** DAVID functional analysis of genes with transcript abundance altered by more than 1.5-fold. **c** Differential isoform usage (left) and major isoforms (right) from the *ELOB* (upper panel) and *PSMB5* (lower panel). Red box: alternative splicing region. **d** Representative RT-PCR analysis of three experiments of alternative splicing events from *ELOB* and *PSMB5* in KGN cells following transfection with siRNAs for *HNRNPH2* or *HNRNPM* (200 nM) and 5'-tRH-Gly<sup>GCC</sup> mimics (50 nM). The arrow indicates the positions and directions of the primers used to amplify the relevant fragments. Red boxes indicate alternate exons, and their neighbouring exons are shown as blank boxes. The bar graph represents a densitometric analysis of the assay (short isoform/long isoform ratio). Values are presented as the mean  $\pm$  S.E.M ( $n = 3$ ).  $P$ -values were obtained by one-way ANOVA

with Dunnett's multiple comparisons test. **e** Validation of alternative splicing events from *ELOB* and *PSMB5* in KGN cells transfected with 5'-tRH-Lys<sup>CTT</sup> or 5'-tRH-Gly<sup>GCC</sup> mimics (50 nM) by RT-qPCR. **f** Validation of alternative splicing events from *ELOB* and *PSMB5* in WT or IRE1 $\alpha$ -knockout (IRE1 $\alpha^{-/-}$ ) KGN cells treated with TM (1  $\mu$ g/mL). The expression of IRE1 $\alpha$  and GAPDH (loading control) was analysed by western blotting (WB). The ribonucleolytic activity of IRE1 $\alpha$  was confirmed by XBPI splicing assay using RT-PCR analysis of unspliced/spliced (u/s) XBPI. **g, h** Validation of the inhibitory effects of AuNP-conjugated ASOs (anti-5'-tRH-Lys<sup>CTT</sup> or anti-5'-tRH-Gly<sup>GCC</sup>) on alternative splicing events of *ELOB* and *PSMB5* was performed using tumour samples obtained from xenograft mice in Fig. 5g (**g**) or Fig. 5i (**h**). The relative abundances of the mRNAs were normalized to that of control mRNAs (set as 1; dot lines). In **e–h**, values are presented as the mean  $\pm$  S.E.M ( $n = 9$ ).  $P$ -values were obtained by unpaired two-tailed  $t$ -test. Source data are provided as a Source Data file.

fragments, the size of which were similar to 5'-tRH-Gly<sup>GCC</sup>, were not detected (Supplementary Fig. 9d). Moreover, primer extension analysis indicates that 5'-tRH-Gly<sup>GCC</sup> fragments in the mouse ovary resulted from the overlapping IRE1 $\alpha$  cleavage site identified in KGN cells, which generates a 33-nt long 5'-tRH-Gly<sup>GCC</sup> (Fig. 7b). To investigate further whether 5'-tRH-Gly<sup>GCC</sup> production is dependent on IRE1 $\alpha$  expression, we utilized mouse B16-BL6 cells since *Ire1a* knockout mice are not available. As shown in Fig. 7c, we observed high levels of 5'-tRH-Gly<sup>GCC</sup> coinciding with enhanced IRE1 $\alpha$  expression when ER stress was induced by TG treatment. Furthermore, we did not observe TG-induced production of 5'-tRH-Gly<sup>GCC</sup> in IRE1 knockdown cells (si-Ire1 $\alpha$ ) (Fig. 7c). These results indicate that ER stress induces selective generation of 5'-tRH-Gly<sup>GCC</sup> in mice in an IRE1 $\alpha$  expression-dependent manner.

We also observed that high levels of 5'-tRH-Gly<sup>GCC</sup> coincided with enhanced IRE1 expression in *C. neoformans* when ER stress was induced by TM treatment (Fig. 7d and Supplementary Fig. 9e). Primer extension analysis indicates that these 5'-tRH-Gly<sup>GCC</sup> resulted from Ire1 cleavage at the site corresponding to the overlapping site identified in KGN cells and mouse ovary (Fig. 7e). A minor band, which was slightly longer than 5'-tRH-Gly<sup>GCC</sup>, was detected in the *ire1*-deletion strain when treated with TM (Fig. 7d and Supplementary Fig. 9e). These results indicate the existence of an additional unknown activity for tRNA<sup>Gly(GCC)</sup> cleavage under ER stress in this yeast species. Taken together, IRE1 $\alpha$ -dependent selective generation of 5'-tRH-Gly<sup>GCC</sup> under ER stress appears to be widely conserved in eukaryotic organisms.

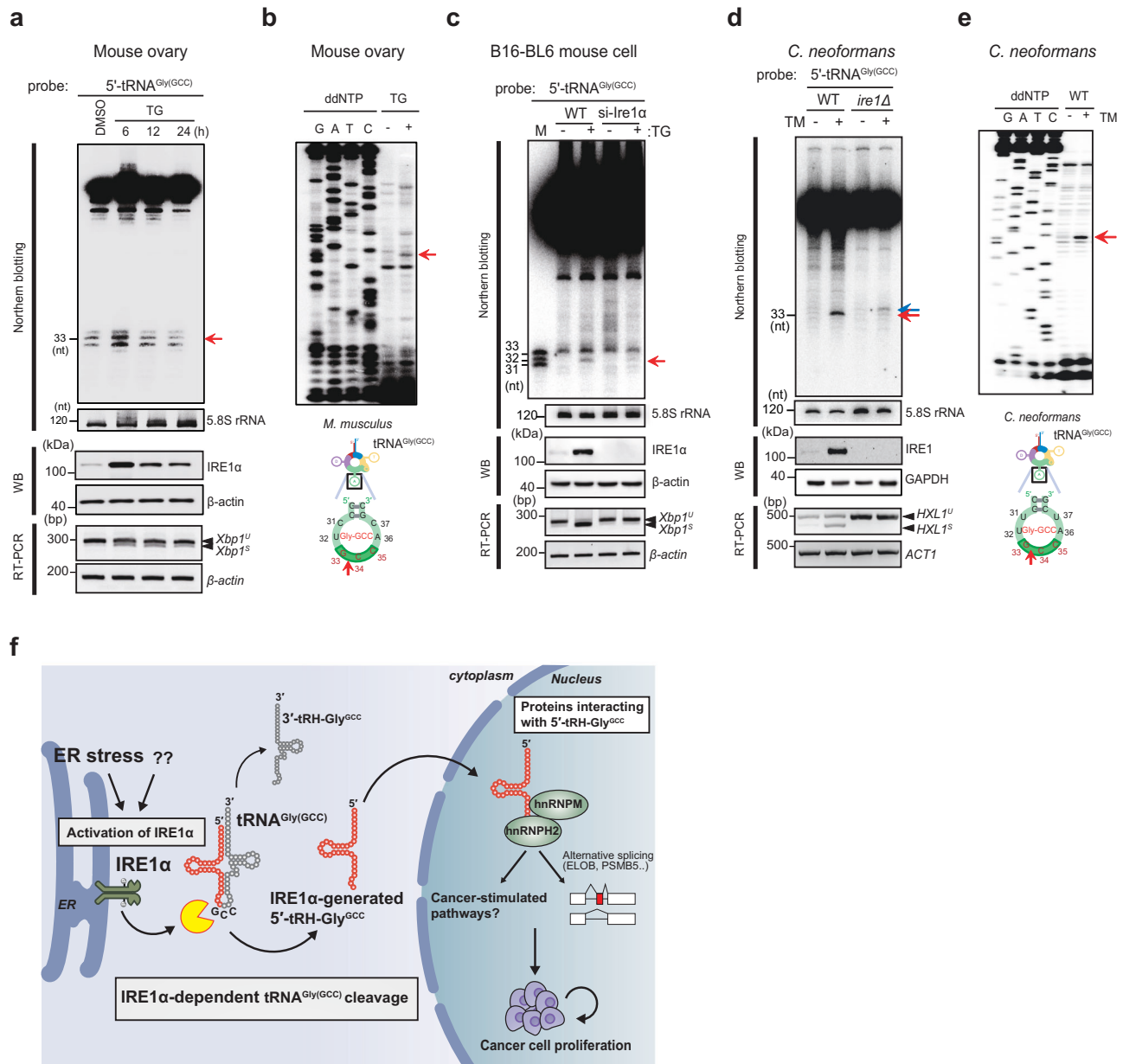


**Fig. 7 | ER stress induces generation of 5'-tRHs from tRNA<sup>Gly(GCC)</sup> in mouse and *C. neoformans*.** **a** Northern blot analysis of tRNA<sup>Gly(GCC)</sup>-derived fragments in the ovary from ER stress-induced mouse. Mice were injected intraperitoneally with control (PBS containing 2% DMSO), TG (1 μg/g body weight) or TM (0.5 μg/g body weight) solution as described in the Methods section. 5.8S rRNA was used as the loading control. **b** (Upper) 5'-end of tRNA<sup>Gly(GCC)</sup> fragment as determined by primer extension assay using total RNA isolated from ovaries after treatment with 0.1% DMSO or TG (0.1 μM) for 6 h. (Lower) Secondary structure of mouse mature tRNA<sup>Gly(GCC)</sup> and IRE1α cleavage sites at anticodon stem loop. Red arrow: TG-induced IRE1α cleavage sites. **c** Northern blot analysis of tRNA<sup>Gly(GCC)</sup> fragments in control B16-BL6 mouse cell (WT) or IRE1α knockdown-B16-BL6 mouse cell (si-Ire1α). Total RNA was isolated and probed with a probe specific for the tRNA<sup>Gly(GCC)</sup>. In **a** and **c**, the expression of IRE1α and β-actin (loading control) was analysed by western blotting (WB). Ribonucleolytic activity of IRE1α was confirmed XBP1 splicing assay using RT-PCR

analysis of unspliced/spliced (u/s) XBP1. Red arrow: tRHs from tRNA<sup>Gly(GCC)</sup> cleaved by IRE1α. **d** Northern blot analysis of tRNA<sup>Gly(GCC)</sup> fragments from WT and *ire1*-deletion (*ire1Δ*) *C. neoformans* treated or not treated with TM (5 μg/ml). Total RNA was isolated and probed with a probe specific for the tRNA<sup>Gly(GCC)</sup>. 5.8S rRNA was used as the loading control. The expression of IRE1 and GAPDH (loading control) was analysed by WB. Ribonucleolytic activity of IRE1 was confirmed HXL1 splicing assay using RT-PCR analysis of unspliced/spliced (u/s) HXL1. Arrows: TM-induced IRE1 cleavage sites. **e** (Upper) Primer extension analysis of tRNA<sup>Gly(GCC)</sup> fragments in *C. neoformans* treated or not treated with TM (5 μg/ml) for 2 h. (Lower) Secondary structure of *C. neoformans* mature tRNA<sup>Gly(GCC)</sup> and IRE1 cleavage sites at anticodon stem loop are illustrated. Red arrow: TM-induced IRE1 cleavage sites. **f** Proposed model for the IRE1α selective generation of 5'-tRH-Gly<sup>GCC</sup> that contributes to cellular adaptation upon ER stress presented in diverse eukaryotic organisms from yeast to humans. Source data are provided as a Source Data file.

## Discussion

This study highlights that IRE1α-mediated selective cleavage of tRNA<sup>Gly(GCC)</sup> and 5'-tRH generation upon ER stress is conserved in human, mice, and a distantly related yeast species, *C. neoformans*. In fact, within these organisms, IRE1α homologues selectively cleave tRNA<sup>Gly(GCC)</sup> species at the same site. These results raise the question of

why these organisms evolutionarily retain this biological event in response to ER stress. Perhaps, as we found in the case of human cancer cells (Figs. 3, 5, and Supplementary Fig. 7), 5'-tRH-Gly<sup>GCC</sup> contributes to cellular adaptation upon ER stress.

Dicer and ANG generate different types of tRFs for multiple roles in cellular processes<sup>35</sup>. However, ANG is the only identified enzyme

associated with the generation of 5'-tRHs by cleaving the anticodon stem-loop of mature tRNAs in mammalian cells<sup>2-5,17,36</sup>. Additional enzymes responsible for the generation of certain 5'-tRHs have not been identified under specific conditions, such as metabolic diseases, cancer, and reproductive cell maturation<sup>18-20</sup>. One such example is 5'-tRH from tRNA<sup>Gly(GCC)</sup> produced in mouse sperm, which reportedly suppresses the expression of genes associated with endogenous retroelement MERVL in embryonic stem cells and embryos by regulating gene expression from specific regions of the genome<sup>19,20</sup>. This 5'-tRH from tRNA<sup>Gly(GCC)</sup> was shown to be upregulated in papillary thyroid carcinoma<sup>18</sup>. Although an increasing number of reports have revealed that tRNA-derived fragments are involved in various biological processes, its biogenesis remains largely unknown. Here, we show that under ER stress conditions, IRE1 $\alpha$  cleaves the anticodon stem-loop of tRNA<sup>Gly(GCC)</sup> to produce 5'-tRH in several human cancer cells. Moreover, generation of 5'-tRHs from tRNA<sup>Gly(GCC)</sup> appears to be ER stress-specific, as it was not related to ANG expression, tRNA modifications such as 5-methylcytosine (m<sup>5</sup>C) deposited by DNMT2 and NSUN2, or other stress conditions tested in this study (Supplementary Figs. 3e-j, 10a-c). Considering our results showing inhibition of cancer cell proliferation and tumour growth by anti-5'-tRH-Gly<sup>GCC</sup> (Fig. 5f-j and Supplementary Fig. 7k, l), these cancer cells might have increased IRE1 $\alpha$  activity involving ER stress. However, since various physiological stimuli other than ER stress can also affect IRE1 $\alpha$  activity, further studies are needed.

Colicins and ANG generate tRHs by cleaving target tRNAs and the anticodon loop of most tRNAs, respectively, thereby inhibiting protein synthesis<sup>37,38</sup>. In the case of IRE1 $\alpha$ -mediated generation of tRHs from tRNA<sup>Gly(GCC)</sup>, it is unlikely that 5'-tRH-Gly<sup>GCC</sup> affects protein synthesis efficiency, as IRE1 $\alpha$  appears to cleave a small portion of tRNA<sup>Gly(GCC)</sup> upon ER stress, and thus, does not significantly reduce the pool of mature tRNA<sup>Gly(GCC)</sup> (Figs. 1c and 2a). Consistent with this notion, overexpression of IRE1 $\alpha$  did not affect expression levels of two glycine-rich proteins, which contain a high proportion of the GGC codon in their mRNA (Supplementary Fig. 10d, Supplementary Table 6).

IRE1 RNase cleaves *XBPI* mRNA, regulated IRE1-dependent decay (RIDD) substrates, and other non-coding RNAs in a sequence-specific manner<sup>39</sup>. A study involving rigid-body docking of the tRNA<sup>Phe</sup> stem-loop into the IRE1 active site<sup>39</sup> suggests that only one stem-loop binds to the IRE1 RNase dimer, where one RNase domain cleaves the RNA and the other assists in recognition and stabilisation. Our results fit well with this model, where IRE1 $\alpha$  can site-specifically cleave the anticodon stem-loop of tRNA<sup>Gly(GCC)</sup>. In addition, expression of a dimerisation-defective mutant of IRE1 $\alpha$  possessing D123P mutation did not notably affect the levels of the 5'-tRHs-Gly<sup>GCC</sup>, suggesting that IRE1 $\alpha$  oligomerization may induce *trans* RNA recognition by IRE1 $\alpha$  (Supplementary Fig. 11). Further studies are needed to understand detailed mechanism of IRE1 $\alpha$  activity on tRNA-Gly<sup>GCC</sup>; for instance, if it is mechanistically related to RIDD or *XBPI* mRNA intron cleavage, which require different factors. Although the detailed modes of action for most tRFs and tRHs remain unclear, several studies indicate that they can regulate the expression and translational efficiency of endogenous target genes by interacting with binding partners, including cytochrome c, YBX1, PIWI, and the AGO family<sup>5,10,40-43</sup>. In the case of 5'-tRH-Gly<sup>GCC</sup>, we found that they interact with two nuclear proteins, HNRNPM and HNRNPH2 (Fig. 4 and Supplementary Fig. 6, 7), and these interactions are required for 5'-tRH-Gly<sup>GCC</sup> to influence cancer cell proliferation (Fig. 5d, e). Knockdown of HNRNPF or HNRNPH1, other interacting proteins identified by Boskovic et al.<sup>31</sup>, showed similar effects on cancer cell survival, suggesting that 5'-tRH-Gly<sup>GCC</sup> interacts with multiple nuclear proteins to exert these effects.

Diverse stresses can induce generation of 5'-tRFs-Gly<sup>GCC</sup> of various lengths that are crucial for cellular functions and stress adaptation<sup>16,18-20</sup>. However, the specific sizes of 5'-tRFs-Gly<sup>GCC</sup> crucial for each specific function remain largely unclear. In the case of our

study, only 33-mer 5'-tRHs-Gly<sup>GCC</sup> was prominently enriched in both RIP-seq samples prepared with immunoprecipitated HNRNPM and HNRNPH2 compared to the input control (Fig. 4d). As neither the full-length tRH-Gly<sup>GCC</sup> nor tRH-Gly<sup>GCC</sup> of sizes other than 33-mer 5'-tRH-Gly<sup>GCC</sup> showed prominent enrichment in HNRNPM or HNRNPH2 RIP-seq samples, we suggest the possibility that HNRNPM and HNRNPH2 recognise a distinct and specific conformation of 5'-tRH-Gly<sup>GCC</sup>. A recent study revealed that hnRNPA2B1 directs the sorting of specific miRNAs into exosomes by recognising a particular short motif<sup>44</sup>.

A recent report identified RBM17, a splicing-related RNA-binding protein, as a binding protein of 5'-tRH-Gly<sup>GCC</sup><sup>18</sup>, supporting our notion that 5'-tRH-Gly<sup>GCC</sup> functions in the nucleus. Our analyses of isoforms within the total transcriptome data using nanopore sequencing, together with the alternative splicing assay results, also indicate that 5'-tRH-Gly<sup>GCC</sup> affects the profiles of a subset of transcript isoforms (Fig. 6). Consistent with these nuclear phenomena, we observed nuclear localisation of 5'-tRH-Gly<sup>GCC</sup> following ER stress (Supplementary Fig. 8). Taken together, our experimental results cohesively indicate that IRE1 $\alpha$ -generated 5'-tRH-Gly<sup>GCC</sup> interacts with HNRNP proteins and affects expression of genes primarily associated with alternative splicing as well as mRNA isoform biogenesis. Considering that HNRNP proteins are known as direct splicing factors, it is hard to mechanistically link alterations in mRNA isoform biogenesis to those in gene expression associated with alternative splicing by 5'-tRH-Gly<sup>GCC</sup>, which is likely to be independently regulated events. However, HNRNP proteins are known to contribute to multiple aspects of gene regulation including alternative splicing, mRNA stabilization, and, transcriptional and translational<sup>45</sup>. Thus, it is possible that 5'-tRH-Gly<sup>GCC</sup> can directly modulate the expression of alternative splicing-associated factors via unknown mechanism. Alternatively, alterations in expression of these factors could be a consequence of the effect of 5'-tRH-Gly<sup>GCC</sup>-HNRNP complexes on mRNA isoform biogenesis. Further studies are needed to elucidate the detailed mechanisms underlying the role of 5'-tRH-Gly<sup>GCC</sup> in alternative splicing events (Fig. 7f).

Aberrant expression of tRNA fragments is reported in various human disease conditions, providing potential targets for disease detection and therapeutics. In addition, recent studies reveal involvement of tRFs in tumorigenesis and cancer development<sup>46-48</sup>. In the case of tRFs derived from tRNA<sup>Gly(GCC)</sup>, Zhang et al. showed that tRFs derived from tRNA<sup>Gly(GCC)</sup> is more abundant in ovarian cancer patients as well as ovarian cancer cell lines. In addition, overexpression of this tRF significantly promoted ovarian cancer cell proliferation<sup>29</sup>. Another study also showed that tRNA<sup>Gly(GCC)</sup>-derived internal fragments (i-tRF-Gly<sup>GCC</sup>) is abundant in ovarian cancer compared to healthy controls<sup>49</sup>. In colorectal cancer (CRC), 5'-tRF-Gly<sup>GCC</sup> is dramatically increased in plasma of CRC patients compared to that of health controls, and these increased levels exhibit a positive correlation with the progression and metastasis of CRC<sup>50</sup>. Li et al., demonstrated that tRNA<sup>Gly(GCC)</sup>-derived small tRNAs were specifically enriched in salivary exosomes of human esophageal squamous cell carcinoma (ESCC) patients, ESCC tissues and ESCC cells, suggesting that these small tRNAs can be used as a non-invasive biomarker for ESCC<sup>51</sup>. Our current study showed that 5'-tRH-Gly<sup>GCC</sup> levels modulate proliferation of several cancer cells in vitro (Fig. 5a-f and Supplementary Fig. 7a, d, g-j). In addition, ASOs-mediated 5'-tRH-Gly<sup>GCC</sup> suppression inhibited tumour proliferation in two xenograft mouse models (Fig. 5g-j). Nonetheless, further investigation is required to fully understand the pathophysiological role of ER stress and IRE1 $\alpha$ -induced 5'-tRHs-Gly<sup>GCC</sup> generation in cancer in general. We believe that understanding the regulatory role of 5'-tRH-Gly<sup>GCC</sup> can be used as a biomarker and potential therapeutic target in cancer cells.

## Methods

### Ethical statement

Our research complies with all relevant ethical regulations. All animal protocols were approved by the Chung-Ang University Institutional Animal Care and Use Committee (IRB# CAU202000115).

### Cell culture and reagents

Cell lines used in this study are described in Supplementary Table 7. DMSO, TG, TM, and STF083010 were purchased from Sigma-Aldrich (St Louis, MO, USA).

### Oligonucleotides

Synthetic oligonucleotides used in this study are listed in Supplementary Table 8.

### Plasmid construction and transfection

Plasmids used in this study are listed in Supplementary Table 9. The myc-tagged IRE1 $\alpha$  (pCMV-IRE1 $\alpha$ ), and ANG were produced by PCR amplification. The PCR products were digested with *KpnI* and *NodI* for IRE1 $\alpha$  and *EcoRI* and *Sall* for ANG (Takara Bio, Shiga, Japan) and then ligated into pCMV-myc empty vector (Clontech, Mountain View, CA, USA). Cells were transfected with plasmids for IRE1 $\alpha$ , IRE1 $\alpha$  (K599A, P830L, and D123P) and ANG using Neon transfection system (Invitrogen, Carlsbad, CA, USA) as described previously<sup>52</sup>. Plasmid encoding Flag-tagged HNRNPH2 (pcDNA3.1(+)-C-DYK-HNRNPH2) and HA-tagged HNRNPM (pcDNA3.1(+)-C-HA-HNRNPM) were synthesised by GenScript (Nanjing, China). Cells were transfected with plasmids for HNRNPH2/M using Lipofectamine 2000 (Invitrogen), according to the manufacturer's instructions.

### Small RNA sequencing analysis

tRNA was sequenced from three biological replicate samples. Total RNA from the KGN and KGN-IRE1 $\alpha^{\text{oe}}$  cells were isolated and treated with T4 polynucleotide kinase (T4 PNK; New England Biolabs, Ipswich, MA, USA) and incubated at 37 °C for 30 min. Samples were separated on a 12% polyacrylamide gel containing 8 M urea to excise the 18–40 nt region and were visualised with SYBR Gold (Thermo Fisher Scientific, Wilmington, DE, USA). RNAs were eluted from the acrylamide bands overnight in 0.3 M NaCl and then precipitated in ethanol/glycogen. Small RNA libraries were constructed using a SMARTer<sup>®</sup> smRNA-Seq Kit for Illumina<sup>®</sup> (Illumina, San Diego, CA, USA) according to the manufacturer's guidelines. Sequencing libraries were generated according to the MiSeq reagent kit v3 and single end sequencing manufacturer instructions. Small RNA-seq reads were trimmed with the cutadapt programme<sup>53</sup> with parameters recommended by the SMARTer smRNA-Seq Kit manual. Trimmed sequences with read-lengths ranging from 25 to 42 bp were collected and mapped to the human genome and non-redundant mature tRNA sequences using the bowtie2 program<sup>52</sup> implemented in the tRAX software package (<http://trna.ucsc.edu/tRAX/>). Reads mapped to tRNAs were extracted and their aligned positions were obtained using the bam2bed program of the BEDOPS suite<sup>53</sup>. The final position of a read was considered a cleavage site. Number of reads ending at each position of tRNAs was calculated. When a read was mapped to multiple tRNAs, it was assigned to a group consisting of matched tRNAs. The resulting read counts were subjected to differential cleavage analysis using the DESeq2 package<sup>54</sup>. We used a tRNA gene annotation format, such as 'W-X:Y<sup>Z</sup>' (W: amino-acid; X: anticodon; Y: cleavage site; Z: unique gene identifier) in Gly-GCC:33<sup>1</sup>.

### Northern blot analysis

The procedure for northern blot analysis has been described previously<sup>55</sup>. In brief, 10–15 micrograms of total RNA sample were denatured at 65 °C for 10 min in an equal volume of formamide loading buffer and loaded onto an 12% polyacrylamide gel containing 8 M urea. RNA was transferred to an Immobilon Hybond-XL membrane (GE Healthcare Life Sciences, Amersham, Buckinghamshire, UK) and then hybridised with a <sup>32</sup>P-5'-end-labelled probe specific for the tRNA<sup>Gly(GCC)</sup>. The northern blot membranes were then stripped and reprobed with a radiolabelled probe specific for the tRNA<sup>Cys(GCA)</sup>, tRNA<sup>Gly(TCC)</sup>, tRNA<sup>Lys(CTT)</sup>, tRNA<sup>Val(TAC)</sup>, or 5.8S rRNA. 5.8S rRNA was used as a loading control.

### Western blot analysis

Total proteins were extracted and analysed by western blotting as described previously<sup>56</sup>. Cell lysates were prepared and subjected to sodium dodecyl sulfate-polyacrylamide gel electrophoresis (SDS-PAGE) for subsequent immunoblotting with the respective antibodies. The protein signals on the membranes were detected using a ChemiDoc XRS + System Imager (Bio-Rad Laboratories, Hercules, CA, USA), and the intensity of each band was quantified using Quantity One software (Bio-Rad Laboratories). For all immunoblot images presented in this manuscript, the membrane was sectioned according to the estimated molecular weights of the proteins of interest and probed with the indicated antibodies. All cropped blots were processed under the same experimental conditions. Total protein from yeast cells was analysed according to the method described by Bahn et al.<sup>57</sup>. The antibodies used in western blot analysis are listed in Supplementary Table 10.

### Primer extension analysis

Three micrograms of total RNA from KGN cells were used in primer extension reactions. The Gly-GCC-R primer was labelled at the 5'-end with ( $\gamma$ -<sup>32</sup>P) ATP and T4 polynucleotide kinase (New England Biolabs). RNA and the labelled primers were denatured at 70 °C for 5 min and then annealed by cooling to 37 °C for 90 min. They were then extended at 42 °C for 1 h with 5 units (U) of avian myeloblastosis virus reverse transcriptase (AMV RTase; New England Biolabs). The products were separated on 10% polyacrylamide gel containing 8 M urea. Sequencing ladders were generated using 5  $\mu$ g of the PCR product amplified from the cDNA of tRNA<sup>Gly(GCC)</sup>. Images were analysed in a Bio-Rad phosphorimager using Quantity One software (Bio-Rad Laboratories).

### tRNA purification

Unfractionated tRNAs (tRNA<sup>Mix</sup>) were purified from total RNA by gel purification. In brief, total RNA from KGN cells was separated on 10% polyacrylamide gel containing 8 M urea. The tRNA fraction was eluted from the gel in RNA extraction buffer [0.5 M ammonium acetate, 0.2% sodium dodecyl sulphate, and 0.1 mM EDTA (pH 8.0)]. The eluted tRNA<sup>Mix</sup> was purified by phenol/chloroform extraction and ethanol precipitation. For further isolation of tRNA<sup>Gly(GCC)</sup>, oligo DNA-immobilised beads were prepared according to the method described by Yokogawa et al.<sup>58</sup>.

### Cleavage analysis and site mapping

Purified total tRNA<sup>Mix</sup> (1  $\mu$ g) and 5'-end <sup>32</sup>P-labelled tRNA<sup>Gly(GCC)</sup> were incubated with 10 pmol of recombinant IRE1 $\alpha$  (OriGene Technologies, Rockville, MD, USA) in 20  $\mu$ L of cleavage buffer [0.2 M HEPES pH 7.6, 0.5 M K(OAC), 10 mM Mg(OAC)<sub>2</sub>, 0.5% Triton X-100, 10 mM DTT, and 10 mM ATP] at 37 °C for 30 or 120 min. The cleaved products from purified tRNA<sup>Mix</sup> were recovered and used for northern blot and primer extension assays. A hydrolysis ladder was then created by incubating 2 pmol of tRNA<sup>Gly(GCC)</sup> in hydrolysis buffer (50 mM NaCO<sub>3</sub> pH 9.2 and 1 mM EDTA pH 8.0) at 95 °C for 10 min. RNase T1 ladder was created by incubating 2 pmol of tRNA<sup>Gly(GCC)</sup> with RNase T1 (Fermentas, Waltham, MA, USA) at 37 °C for 2 min in reaction buffer (30 mM Tris-HCl pH 7.9, 10 mM MgCl<sub>2</sub>, 160 mM NaCl, 0.1 mM DTT, and 0.1 mM EDTA pH 8.0). The cleaved products from radiolabelled tRNA<sup>Gly(GCC)</sup> were separated on a 10% polyacrylamide gel containing 8 M urea, and images were analysed in a Bio-Rad phosphorimager using the Quantity One software (Bio-Rad Laboratories).

### Semi-quantitative RT-PCR and Reverse transcription-quantitative real-time PCR (RT-qPCR)

To amplify the spliced and unspliced *XBPI* mRNA, a pair of primers (*XBPI* splicing-F and *XBPI* splicing-R) were used to flank the splicing site and yield 473 bp and 447 bp product sizes of *XBPIu* and *XBPIs*, respectively. Products were resolved on 2.5% agarose gel. Alternative

splicing was detected using isoform specific primers. To amplify the spliced and unspliced *HXLI* mRNA, a pair of primers, C. deuterio-F and C. deuterio-R, were used as described previously<sup>59</sup>, yielding PCR product sizes of 475 bp and 419 bp for *HXLIu* and *HXLIs*, respectively. These PCR products were electrophoresed on 2.5% agarose gel. *ACT1* was used as a loading control. Samples for RT-qPCR was prepared and analysed as previously described<sup>56</sup>. Gene expression levels were quantified using the  $\Delta\Delta C_t$  method. Primers used in this study are listed in Supplementary Table 8.

### Construction of IRE1 $\alpha$ or ANG KO cell line

IRE1 $\alpha$  or ANG KO KGN cells were generated as described previously<sup>56</sup>. In brief, to generate plasmids targeting IRE1 $\alpha$ , pX458 (D10A)-IRE1 $\alpha$  (Guide A) or pX458 (D10A)-IRE1 $\alpha$  (Guide B) dual-guide oligonucleotide primers were cloned into the vector pX458 (D10A). To generate plasmids targeting ANG, pX458 (D10A)-ANG (Guide A) or pX458 (D10A)-ANG (Guide B) dual-guide oligonucleotide primers were cloned into the vector pX458 (D10A). KGN cells ( $1 \times 10^6$ ) were cultured in 100-mm dishes and transfected with 5  $\mu$ g of CRISPR plasmids. The transfected cells were cultured for 24 h, harvested, and resuspended in phosphate buffered saline (Ca<sup>2+</sup>/Mg<sup>2+</sup>-free, 1 mM EDTA, 25 mM HEPES pH 7.0, and heat-inactivated 1% FBS). The cells were then sorted, based on GFP signal, by flow cytometry using the BD FACSAria II cell sorter (BD Bioscience, USA). Cells were sorted into the individual wells of 96-well plates and then expanded further. Allelic deletion was confirmed by TOPcloner™ TA core Kit (Enzynomics, Daejeon, Korea) and DNA sequencing (Cosmogenetech, Seoul, Korea).

### Oligonucleotide pull-down assay

KGN cells were treated for 6 h with 0.1  $\mu$ M TG; untreated cells were included as controls. After washing twice with 1 $\times$  PBS, harvested cells were disrupted with ice-cold cell lysis buffer [4% CHAPS, 100 mM NaCl, 2 mM EDTA and a 1 $\times$  protease inhibition cocktail (Roche, Mannheim, Germany) in 50 mM Tris/HCl buffer, pH 7.2]. To capture proteins bound to the enriched 5'-tRH-Gly<sup>CCC</sup> from TG-treated cells, 34 nucleotide RNA baits (200 nM each), designed via biotinylation of the 5'- or 3'-end were utilised in a Thermo Scientific Pierce streptavidin-coated microplate containing 200-500  $\mu$ g protein per well and an RNase inhibitor (Promega). A 5'-biotin-oligo A8 RNA was included in control. Following incubation for 1 h at 4 °C, the contents of the protein extract were aspirated and washed with 100 mM, 300 mM, and 500 mM NaCl in 25 mM Tris/HCl (pH 7.2). The bound proteins were eluted with SDS-PAGE loading buffer containing 1% (w/v) SDS and 5% (v/v) 2-mercaptoethanol, as well as 10% (v/v) glycerol in 25 mM Tris/HCl (pH 6.8).

HNRNPM or HNRNPH2 were pull-downed upon precipitation of 5'-biotin-labelled 5'-tRH-Gly<sup>CCC</sup> probes using the same method as described above, except the protein extract were aspirated and washed with 1 $\times$  PBS-T and then the bound proteins were prepared with 6 $\times$  SDS loading buffer for western blot assay. The cellular levels of IRE1 $\alpha$ , HNRNPM, HNRNPH2 and  $\beta$ -actin were determined by western blotting.

### RNA immunoprecipitation sequencing (RIP-seq)

RNA immunoprecipitation was performed as described in a previous study<sup>60</sup>. Briefly, the A2058 cells ( $2 \times 10^6$ ) were transfection with 2  $\mu$ g of each plasmid (Myc-IRE1 $\alpha$ , Flag-HNRNPH2, HA-HNRNPM) for 24 h. A total of 40 plates (100 mm) of the transfected cells were used for each immunoprecipitation experiment. Cells were washed twice with cold PBS and resuspended in 400  $\mu$ l RIP lysis buffer supplemented with protease inhibitor cocktail and RNase inhibitor, and snap frozen to -80 °C. Then, 100  $\mu$ l of Protein G magnetic beads (Thermo Fisher Scientific) and 10  $\mu$ g each Tag (Flag or HA) or control mouse IgG (Santa Cruz Biotechnology, Santa Cruz, CA, USA) were rotated and incubated at room temperature for 4 h to allow binding of the antibody to the

magnetic beads. Then the 100  $\mu$ l cell lysates and the antibody bound with magnetic beads were rotated and incubated at 4 °C overnight. RNA was eluted from magnetic beads using Proteinase K, followed by extraction with the phenol-chloroform method and treatment with T4 PNK (New England Biolabs) at 37 °C for 30 min. Small RNA (<200 nt) was isolated using the mirVana miRNA isolation kit (Invitrogen) according to the manufacturer's instructions. Sequencing libraries were constructed using the SMARTer® smRNA-Seq kit for Illumina (Takara Bio) according to manufacturer's instructions. The generated libraries were sequenced using a MiniSeq system (Illumina) for high-throughput sequencing.

### Tandem mass spectrometry analysis

Protein bands detected via SDS-PAGE, following the biotin-streptavidin method, were excised, destained, and reduced with 50 mM dithiothreitol at 60 °C for 15 min. The reduced cysteine residues were alkylated with 100 mM iodoacetamide at room temperature for 1 h in the dark. The gel pieces were then washed twice with deionised water and dehydrated twice in acetonitrile (ACN). The dried gels were soaked in 10 mM ammonium bicarbonate with 20  $\mu$ g/mL trypsin (Promega, Madison WI, USA) on ice. Proteins in gel were digested for 24 h at 37 °C and treated again with 20  $\mu$ l of trypsin solution for another 24 h. The digested peptides were extracted from the gel pieces and analysed on an nLC Velos Pro mass instrument equipped with a PicoFrit™ column (100 mm, packed with 5  $\mu$ m Biobasic® C18) and an EASY-Column™ (2 cm, packed with 5  $\mu$ m C18; Thermo Fisher Scientific). The LC conditions were as follows: 0.3  $\mu$ l/min was a 45-min linear gradient from 5% to 40% ACN in a 0.1% formic acid buffer solution, followed by a 10 min column wash with 80% ACN and 20 min re-equilibration to the initial buffer condition. Full mass (MS1) scan was performed in the  $m/z$  300–2000 range in a positive ion mode. Data-dependent MS2 scans of the seven most intense ions were performed from the full scan with the options of 1.5  $m/z$  isolation width, 35% normalised collision energy, and 30 s dynamic exclusion duration. The acquired MS2 data were primarily analysed by SEQUEST search against a human reference protein database from the National Center for Biotechnology Information (<https://www.ncbi.nlm.nih.gov/genome>) and common protein contaminants in the common Repository of Adventitious Proteins (<https://www.thegpm.org/crap/>) with the following options: maximum miscleavage of 1, precursor mass tolerance 0.8 Da, fragment mass tolerance 1.0 Da, dynamic modification of methionine oxidation, and static modification of cysteine with iodoacetamide. The identified proteins with unique peptides are reported in Supplementary Table 2.

### Electrophoretic mobility shift assay (EMSA)

The synthetic full-length tRNAs and 5'-tRH-mimics were purchased from Bioneer (Daejeon, Korea) and synthetic ASOs or 5'-tRHs were purchased from Cosmogenetech. The 5'-end of tRH mimics were radiolabelled using  $\gamma$ -<sup>32</sup>P-ATP and T4 polynucleotide kinase (Takara Bio) and purified with an Illustra MicroSpin G-25 column (GE Healthcare Life Sciences). Prior to use, labelled and unlabelled tRH mimics were heated at 65 °C for 10 min and slowly cooled to room temperature. Next, 100 ng of BSA (Takara Bio), or HNRNPM (Mybiosource, San Diego, USA) or HNRNPH2 recombinant proteins (Mybiosource), were incubated with binding buffer [10 mM Tris-HCl (pH 8.0), 150 mM KCl, 0.5 mM EDTA, 0.1% Triton X-100, 0.02 mM DTT, 12.5% glycerol] and 3.3 pmol of cold probes for each 5'-tRH mimic for 10 min at room temperature. Samples were then incubated with 0.033 pmol of 5'-labelled tRHs for 10 min at room temperature. Native loading dye [100 mM Tris-HCl (pH 8.0), 8.33% glycerol, 0.002% brilliant blue G] and 8% polyacrylamide gels were used to load the samples. Vacuum dried gels were exposed to an intensifying screen and images were analysed in a Bio-Rad phosphorimager using Quantity One software (Bio-Rad Laboratories).

For analysis of specific interactions between ASOs and 5'-tRH, all the full-length tRNAs (tRNA<sup>Gly(GCC)</sup> or tRNA<sup>Lys(CTT)</sup>), 5'-tRHs (5'-tRH-Gly<sup>GCC</sup> or 3'-tRH-Gly<sup>GCC</sup>) and ASOs (anti-5'-tRH-Gly<sup>GCC</sup> or anti-3'-tRH-Gly<sup>GCC</sup>) were heated to 65 °C for 10 min and slowly cooled to room temperature. Followed by refolding procedure, 7 pmol of each full-length tRNAs or 5'-tRHs were mixed with the designated number of ASOs and incubated at 37 °C for 15 min in triple distilled water. Then the samples were mixed with 6× native RNA loading dye [1× TBE, 12% glycerol, 0.085% xylene cyanol, 0.085% BPB] and electrophoresed in 12% non-denaturing polyacrylamide gel under 1× TB buffer. The gels were stained by SYBR™ Gold Nucleic Acid Gel Stain (Invitrogen), and imaged with Amersham ImageQuant 800 (Cytiva, Marlborough, MA, USA).

### HNRNPM and HNRNPH2 binding constants

The binding affinities of purified HNRNPM and HNRNPH2 (Mybio-source, San Diego, USA) to synthetic 5'-tRH-Gly<sup>GCC</sup> or 3'-tRH-Gly<sup>GCC</sup> were measured using BIAcore T200 instrument and CM5 sensorchip (GE Healthcare Life Sciences) at 25 °C. Activation, immobilization, deactivation and preparation of the mock-coupled flow cell were performed according to the manufacturer's instructions. The binding signals were generated by subtracting the signal for the mock-coupled flow cell from that for the HNRNPM- or HNRNPH2-immobilized flow cells. Calculation of equilibrium dissociation constant ( $K_D$ ) from the sensorgrams were done with BIAcore T200 Evaluation software version 3.2 (GE Healthcare Life Sciences) by fitting the data to a 1:1 binding model.

### Cell viability assay

All tRH mimics were purchased from were supplied by Genolution Pharmaceuticals, Inc. (Seoul, Korea). ASOs were purchased from BIO-NICS (Seoul, Korea). Cell-viability assays were performed as previously<sup>56</sup>. In brief, Cells ( $1 \times 10^4$ ) were seeded in 96-well plates for 24 h; the cells were then transfected with increasing amounts of mimics or ASOs using the lipofectamine 2000 reagent (Invitrogen).

### Cell proliferation assay

Cells ( $1 \times 10^4$ ) were seeded in 96-well plates for 24 h; the cells were then transfected with increasing amounts of 5'-tRH-Gly<sup>GCC</sup>, 5'-tRH-Lys<sup>CTT</sup>, or scrambles using the lipofectamine 2000 reagent (Invitrogen). HeLa or A2058 cells ( $1 \times 10^4$ ) were seeded in 96-well plates for 24 h; the cells were then transfected with increasing amounts of ASOs complementary to the 5'-tRH-Gly<sup>GCC</sup> or 5'-tRH-Lys<sup>CTT</sup> loaded onto functionalized AuNP. After a 48 h transfection, cell proliferation was measured using the Cell Proliferation ELISA, BrdU (colorimetric) kit (Sigma-Aldrich) according to the manufacturer's instructions.

### Flow cytometry analysis

To detect apoptotic cells, KGN cells ( $1 \times 10^6$ ) were transfected with the indicated 5'- or 3'-tRHs mimic and 48 h post-transfection stained with the FITC Annexin V Apoptosis Detection Kit (BD Pharmingen, San Diego, CA, USA) according to the manufacturer's instructions.

### Cell migration assay

Cell migration was assessed based on the protocol described in our previous study<sup>56</sup>. Briefly, KGN cells ( $1 \times 10^6$ ) were transfected with the indicated 5'- or 3'-tRH mimics for 48 h. Images of migrated cells were captured at ×100 magnification under a bright-field microscope (Olympus CKX41, Tokyo, Japan).

### Total transcriptome analysis

RNA was sequenced from two biological replicate samples of KGN cells transfected with the 5'-tRHs mimic for 48 h. In brief, total RNA samples were converted into cDNA libraries using the TruSeq Stranded mRNA Sample Prep Kit (Illumina). Starting with 1 µg of total RNA, polyadenylated RNA (primarily mRNA) was selected and purified using

oligo-dT-conjugated magnetic beads. This mRNA was physically fragmented and converted into single-stranded cDNA using reverse transcriptase and random hexamer primers, with the addition of actinomycin D to the FSA (First Strand Synthesis Act D Mix) to suppress DNA-dependent synthesis of the second strand. Double-stranded cDNA was created by removing the RNA template and synthesising the second strand in the presence of dUTP (deoxyribouridine triphosphate) in place of dTTP (deoxythymidine triphosphate). A single A base was added to the 3' end to facilitate ligation of the sequencing adaptors, which contained a single T base overhang. Adaptor-ligated cDNA was amplified by PCR to increase the amount of sequence-ready library. During this amplification the polymerase stalls when it encounters a U base, rendering the second strand a poor template. Accordingly, amplified material uses the first strand as a template, thereby preserving the strand information. Final cDNA libraries were analysed for size distribution using an Agilent Bioanalyzer (DNA 1000 kit; Agilent), quantitated by qPCR (Kapa Library Quant Kit; Kapa Biosystems, Wilmington, MA), and normalised to 2 nmol/L in preparation for total transcriptome analysis.

### Alternative splicing analysis

Purified mRNA was sequenced from three biological triplicate samples of KGN cells transfected with the 5'-tRHs mimic for 48 h. Briefly, Direct RNA sequencing was performed using the Direct RNA sequencing protocol (SQK-PCS109 kit) for the MinION. All steps were followed according to the manufacturer's specification. The constructed library was loaded on a FLO-MINIO6D R9.4 flow cell and sequenced on a MinION device (Oxford Nanopore Technologies). The sequencing run was terminated after 48 h. Analyses of differential isoform usage using FLAIR modules has been described previously<sup>33</sup>.

### Induction of acute ER stress in vivo

Acute ER stress was induced in vivo using a mouse model as described previously<sup>34</sup>. Briefly, immunodeficient female or male BALB/c nu/nu mice (7-weeks-old) were purchased from Saeron Bio Inc (Uiwang, Korea) and rested for 3–5 days. BALB/c mice were injected intraperitoneally with TG solution (1 µg/g body weight) or TM solution (0.5 µg/g body weight) as described previously. As controls, mice were injected intraperitoneally with control buffer (1× PBS containing 2% DMSO). Mice were euthanized by cervical dislocation and, major organs were harvested at 6 h, 12 h, and 24 h post-treatment, and the samples were prepared for western blot and northern blot analyses. The animal room housing the mice was maintained at a humidity of 30–40%, a temperature of  $22 \pm 1$  °C, and a 12 h light/dark cycle. For *C. neoformans*, WT and *ire1*-deletion (*ire1Δ*) strains in early log phase were treated with TM (5 µg/ml) and DTT (2 mM) at 30 °C for 2 h.

### Fluorescence in situ hybridisation

Cells were cultured under conditions of normal growth or subjected to ER stress by treating with 0.1 µM TG for 6 h. After culture, the cells were washed thrice in PBS, fixed with 4% paraformaldehyde in PBS for 15 min at room temperature, and washed thrice with PBS. Cells were permeabilised with 0.2% Triton X-100 in PBS for 15 min at room temperature and washed twice with PBS. Slides were then blocked and prehybridised for 2 h at 37 °C in hybridisation buffer (2% bovine serum albumin, 5× Denhardt's solution, 4× SSC, and 35% deionised formamide). Hybridisation was performed overnight in a humid dark chamber at 37 °C in the presence of 1 ng/mL of the indicated oligonucleotide conjugated to cyanine 3 dye (Cy3). FISH assays were also performed under denaturing conditions by heating the slides at 75 °C for 5 min, immediately before the hybridisation step. After hybridisation, cells were washed once in 2× SSC containing 50% deionised formamide, once in 2× SSC, and once in 1× SSC. Cells were mounted on slides using a mounting solution containing DAPI. Fluorescence was detected with a laser scanning confocal microscope (Carl Zeiss ZEN

2011, Germany). Relative fluorescence intensities were assessed using ImageJ software (NIH, USA).

### TaqMan assay

The TaqMan assay was performed as described previously<sup>56</sup>. Briefly, cells were treated with TG (0.1  $\mu$ M) or TM (1  $\mu$ g/ml) for the indicated times, and Total RNA was extracted using TRIzol (Invitrogen). For the determine the subcellular distribution of ER-stress induced 5'-tRH-Gly<sup>GCC</sup>, cells were treated with 0.1  $\mu$ M of TG for the indicated times, and fractionation of nuclear and cytosolic RNA was isolated using a Cyttoplasmic and Nuclear RNA Purification Kit (Norgen Biotek, Thorold, Canada), according to the manufacturer's instructions. 5'-tRH-Gly<sup>GCC</sup>, 5'-tRH-Lys<sup>CTT</sup>, and U6 snRNA quantification was conducted using custom designed TaqMan microRNA assays according to manufacturer's recommended protocols (Applied Biosystems, Foster City, CA, USA).

### Mouse xenograft experiment

HeLa cells ( $1 \times 10^6$ ) or A2058 cells ( $2 \times 10^6$ ) were subcutaneously injected into 7-week-old BALB/c nu/nu immunodeficient female mice (Saeron Bio Inc), whose weights ranged between 17 and 18 g. After HeLa cell-derived subcutaneous xenograft reached about 100 mm<sup>3</sup>, mice ( $n=10$  per each group) were treated with AuNP<sup>dT</sup> loaded with anti-scramble, anti-HNRNPM, or anti-HNRNPH2, followed by alternate injections of AuNP<sup>dT</sup> loaded with anti-scramble or anti-5'-tRH-Gly<sup>GCC</sup> every other day. Once the A2058 cell-derived subcutaneous xenograft reached about 100 mm<sup>3</sup>, mice ( $n=12$  per each group) were treated with AuNP<sup>dT</sup> loaded with anti-scramble or AuNP<sup>dT</sup>-anti-5'-tRH-Gly<sup>GCC</sup> were directly injected into the tumour sites every two days. AuNP<sup>dT</sup> loaded with ASOs were prepared by mixing AuNP<sup>dT</sup> (NES Biotechnology, Seoul, Korea) with polyadenylated ASOs as previously described<sup>32</sup>. Mice were weighed and sizes of the tumours were measured every other day. The volume (cm<sup>3</sup>) of each tumour ((length  $\times$  width<sup>2</sup>  $\times$   $\pi$ )/6) was determined over 30 days period after xenotransplantation. Tumour-bearing mice were euthanized by cervical dislocation ~20 days after the first injection of the functionalized AuNP composites, and tumours were excised. The animal room housing the mice was maintained at a humidity of 30–40%, a temperature of  $22 \pm 1$  °C, and a 12 h light/dark cycle. The maximal tumour volume (2000mm<sup>3</sup>) was permitted by the institutional animal care and use committee. The samples were prepared for RT-qPCR and western blot analyses.

### Statistics and reproducibility

All statistical analyses were performed using Graph Pad Prism 9 software (version 9.4.1) (Graph Pad Software Inc.) or SAS version 9.2 (SAS Institute, Cary, NC, USA). Results are expressed as the mean  $\pm$  standard error of the mean (S.E.M) as indicated. Statistical test was chosen on the basis of data distribution normality, which was checked with Shapiro–Wilk test. Two-tailed, unpaired *t*-test, one-way or two-way analysis of variance (ANOVA) followed by post-hoc tests were used to determine significance as indicated in the Figure legends.  $P < 0.05$  was considered statistically significant. Details of the particular statistical analyses used, statistical significance, number of independent biological replicates and sample sizes for all of the graphs are indicated in the Figures or Figure legends. All data is representative of at least three independent experiments with similar results unless otherwise designated. The sample sizes were determined based on previous experimental experience and no statistical method was used to predetermine sample sizes.

### Reporting summary

Further information on research design is available in the Nature Portfolio Reporting Summary linked to this article.

### Data availability

Small RNA-seq data and RIP-seq data was deposited in the NCBI Sequence Read Archive (SRA) under the BioProject accession number [PRJNA772059](https://doi.org/10.1038/s41467-024-53624-4). The mass spectrometry data have been deposited in the ProteomeXchange Consortium via the PRIDE<sup>61</sup> partner repository with the dataset identifier [PXD013798](https://doi.org/10.1038/s41467-024-53624-4). Source data are provided with this paper.

### References

- Kim, H. K., Yeom, J. H. & Kay, M. A. Transfer RNA-Derived Small RNAs: Another Layer of Gene Regulation and Novel Targets for Disease Therapeutics. *Mol. Ther.* **28**, 2340–2357 (2020).
- Fu, H. et al. Stress induces tRNA cleavage by angiogenin in mammalian cells. *FEBS Lett.* **583**, 437–442 (2009).
- Yamasaki, S., Ivanov, P., Hu, G. F. & Anderson, P. Angiogenin cleaves tRNA and promotes stress-induced translational repression. *J. Cell Biol.* **185**, 35–42 (2009).
- Honda, S. et al. Sex hormone-dependent tRNA halves enhance cell proliferation in breast and prostate cancers. *Proc. Natl Acad. Sci. USA* **112**, E3816–E3825 (2015).
- Saikia, M. et al. Angiogenin-cleaved tRNA halves interact with cytochrome c, protecting cells from apoptosis during osmotic stress. *Mol. Cell. Biol.* **34**, 2450–2463 (2014).
- Haussecker, D. et al. Human tRNA-derived small RNAs in the global regulation of RNA silencing. *RNA* **16**, 673–695 (2010).
- Cole, C. et al. Filtering of deep sequencing data reveals the existence of abundant Dicer-dependent small RNAs derived from tRNAs. *RNA* **15**, 2147–2160 (2009).
- Maute, R. L. et al. tRNA-derived microRNA modulates proliferation and the DNA damage response and is down-regulated in B cell lymphoma. *Proc. Natl Acad. Sci. USA* **110**, 1404–1409 (2013).
- Li, Z. et al. Extensive terminal and asymmetric processing of small RNAs from rRNAs, snoRNAs, snRNAs, and tRNAs. *Nucleic Acids Res.* **40**, 6787–6799 (2012).
- Ivanov, P., Emara, M. M., Villen, J., Gygi, S. P. & Anderson, P. Angiogenin-induced tRNA fragments inhibit translation initiation. *Mol. Cell* **43**, 613–623 (2011).
- Gebetsberger, J., Zywicki, M., Künzi, A. & Polacek, N. tRNA-derived fragments target the ribosome and function as regulatory non-coding RNA in *Haloflex volcanii*. *Archaea* **2012**, 260909 (2012).
- Luo, S. et al. Drosophila tsRNAs preferentially suppress general translation machinery via antisense pairing and participate in cellular starvation response. *Nucleic Acids Res.* **46**, 5250–5268 (2018).
- Sobala, A. & Hutvagner, G. Small RNAs derived from the 5' end of tRNA can inhibit protein translation in human cells. *RNA Biol.* **10**, 553–563 (2013).
- Kim, H. K. et al. A transfer-RNA-derived small RNA regulates ribosome biogenesis. *Nature* **552**, 57–62 (2017).
- Lee, Y. S., Shibata, Y., Malhotra, A. & Dutta, A. A novel class of small RNAs: tRNA-derived RNA fragments (tRFs). *Genes Dev.* **23**, 2639–2649 (2009).
- Chen, Z. et al. Transfer RNA demethylase ALKBH3 promotes cancer progression via induction of tRNA-derived small RNAs. *Nucleic Acids Res.* **47**, 2533–2545 (2019).
- Shao, Y. et al. tRF-Leu-CAG promotes cell proliferation and cell cycle in non-small cell lung cancer. *Chem. Biol. Drug Des.* **90**, 730–738 (2017).
- Han, L. et al. A 5'-tRNA halve, tiRNA-Gly promotes cell proliferation and migration via binding to RBM17 and inducing alternative splicing in papillary thyroid cancer. *J. Exp. Clin. Cancer Res.* **40**, 222 (2021).
- Chen, Q. et al. Sperm tsRNAs contribute to intergenerational inheritance of an acquired metabolic disorder. *Science* **351**, 397–400 (2016).



20. Sharma, U. et al. Biogenesis and function of tRNA fragments during sperm maturation and fertilization in mammals. *Science* **351**, 391–396 (2016).
21. Lee, K. P. et al. Structure of the dual enzyme Ire1 reveals the basis for catalysis and regulation in nonconventional RNA splicing. *Cell* **132**, 89–100 (2008).
22. Cox, J. S., Shamu, C. E. & Walter, P. Transcriptional induction of genes encoding endoplasmic reticulum resident proteins requires a transmembrane protein kinase. *Cell* **73**, 1197–1206 (1993).
23. Calfon, M. et al. IRE1 couples endoplasmic reticulum load to secretory capacity by processing the XBP-1 mRNA. *Nature* **415**, 92–96 (2002).
24. Yoshida, H., Matsui, T., Yamamoto, A., Okada, T. & Mori, K. XBP1 mRNA is induced by ATF6 and spliced by IRE1 in response to ER stress to produce a highly active transcription factor. *Cell* **107**, 881–891 (2001).
25. Coelho, D. S. et al. Xbp1-independent Ire1 signaling is required for photoreceptor differentiation and rhabdomyere morphogenesis in *Drosophila*. *Cell Rep.* **5**, 791–801 (2013).
26. Hollien, J. et al. Regulated Ire1-dependent decay of messenger RNAs in mammalian cells. *J. Cell Biol.* **186**, 323–331 (2009).
27. Upton, J. P. et al. IRE1 $\alpha$  cleaves select microRNAs during ER stress to derepress translation of proapoptotic Caspase-2. *Science* **338**, 818–822 (2012).
28. Oikawa, D., Tokuda, M., Hosoda, A. & Iwawaki, T. Identification of a consensus element recognized and cleaved by IRE1 alpha. *Nucleic Acids Res.* **38**, 6265–6273 (2010).
29. Zhang, M. et al. tRNA-derived fragment tRF-03357 promotes cell proliferation, migration and invasion in high-grade serous ovarian cancer. *Onco Targets Ther.* **12**, 6371–6383 (2019).
30. Tirasophon, W., Welihinda, A. A. & Kaufman, R. J. A stress response pathway from the endoplasmic reticulum to the nucleus requires a novel bifunctional protein kinase/endoribonuclease (Ire1p) in mammalian cells. *Genes Dev.* **12**, 1812–1824 (1998).
31. Boskovic, A., Bing, X. Y., Kaymak, E. & Rando, O. J. Control of non-coding RNA production and histone levels by a 5' tRNA fragment. *Genes Dev.* **34**, 118–131 (2020).
32. Kim, J. H. et al. A functionalized gold nanoparticles-assisted universal carrier for antisense DNA. *Chem. Commun.* **46**, 4151–4153 (2010).
33. Tang, A. D. et al. Full-length transcript characterization of SF3B1 mutation in chronic lymphocytic leukemia reveals downregulation of retained introns. *Nat. Commun.* **11**, 1438 (2020).
34. Abdullahi, A., Stanojic, M., Parousis, A., Patsouris, D. & Jeschke, M. G. Modeling Acute ER Stress in Vivo and in Vitro. *Shock* **47**, 506–513 (2017).
35. Kumar, P., Kuscu, C. & Dutta, A. Biogenesis and Function of Transfer RNA-Related Fragments (tRFs). *Trends Biochemical Sci.* **41**, 679–689 (2016).
36. Emara, M. M. et al. Angiogenin-induced tRNA-derived stress-induced RNAs promote stress-induced stress granule assembly. *J. Biol. Chem.* **285**, 10959–10968 (2010).
37. Ogawa, T. et al. A cytotoxic ribonuclease targeting specific transfer RNA anticodons. *Science* **283**, 2097–2100 (1999).
38. Tomita, K., Ogawa, T., Uozumi, T., Watanabe, K. & Masaki, H. A cytotoxic ribonuclease which specifically cleaves four isoaccepting arginine tRNAs at their anticodon loops. *Proc. Natl Acad. Sci. USA* **97**, 8278–8283 (2000).
39. Korennykh, A. & Walter, P. Structural basis of the unfolded protein response. *Annu Rev. Cell Dev. Biol.* **28**, 251–277 (2012).
40. Kumar, P., Anaya, J., Mudunuri, S. B. & Dutta, A. Meta-analysis of tRNA derived RNA fragments reveals that they are evolutionarily conserved and associate with AGO proteins to recognize specific RNA targets. *BMC Biol.* **12**, 78 (2014).
41. Goodarzi, H. et al. Endogenous tRNA-Derived Fragments Suppress Breast Cancer Progression via YBX1 Displacement. *Cell* **161**, 790–802 (2015).
42. Couvillion, M. T., Bounova, G., Purdom, E., Speed, T. P. & Collins, K. A Tetrahymena Piwi bound to mature tRNA 3' fragments activates the exonuclease Xrn2 for RNA processing in the nucleus. *Mol. cell* **48**, 509–520 (2012).
43. Martinez, G., Choudury, S. G. & Slotkin, R. K. tRNA-derived small RNAs target transposable element transcripts. *Nucleic Acids Res.* **45**, 5142–5152 (2017).
44. Villarroya-Beltri, C. et al. Sumoylated hnRNPA2B1 controls the sorting of miRNAs into exosomes through binding to specific motifs. *Nat. Commun.* **4**, 2980 (2013).
45. Geuens, T., Bouhy, D. & Timmerman, V. The hnRNP family: insights into their role in health and disease. *Hum. Genet* **135**, 851–867 (2016).
46. Fu, M. et al. Emerging roles of tRNA-derived fragments in cancer. *Mol. Cancer* **22**, 30 (2023).
47. Zhang, S., Yu, X., Xie, Y., Ye, G. & Guo, J. tRNA derived fragments: A novel player in gene regulation and applications in cancer. *Front. Oncol.* **13**, 1063930 (2023).
48. Gong, M., Deng, Y., Xiang, Y. & Ye, D. The role and mechanism of action of tRNA-derived fragments in the diagnosis and treatment of malignant tumors. *Cell Commun. Signal* **21**, 62 (2023).
49. Panoutsopoulou, K. et al. tRNA(GlyGCC)-Derived Internal Fragment (i-tRF-GlyGCC) in Ovarian Cancer Treatment Outcome and Progression. *Cancers* **14**, 24 (2021).
50. Wu, Y. et al. 5'-tRF-GlyGCC: a tRNA-derived small RNA as a novel biomarker for colorectal cancer diagnosis. *Genome Med* **13**, 20 (2021).
51. Li, K. et al. A signature of saliva-derived exosomal small RNAs as predicting biomarker for esophageal carcinoma: a multicenter prospective study. *Mol. Cancer* **21**, 21 (2022).
52. Langmead, B. & Salzberg, S. L. Fast gapped-read alignment with Bowtie 2. *Nat. methods* **9**, 357–359 (2012).
53. Neph, S. et al. BEDOPS: high-performance genomic feature operations. *Bioinformatics* **28**, 1919–1920 (2012).
54. Love, M. I., Huber, W. & Anders, S. Moderated estimation of fold change and dispersion for RNA-seq data with DESeq2. *Genome Biol.* **15**, 550 (2014).
55. Lee, K., Bernstein, J. A. & Cohen, S. N. RNase G complementation of rne null mutation identifies functional interrelationships with RNase E in *Escherichia coli*. *Mol. Microbiol* **43**, 1445–1456 (2002).
56. Shin, E. et al. An alternative miRISC targets a cancer-associated coding sequence mutation in FOXL2. *EMBO J.* **39**, e104719 (2020).
57. Bahn, Y. S., Kojima, K., Cox, G. M. & Heitman, J. Specialization of the HOG pathway and its impact on differentiation and virulence of *Cryptococcus neoformans*. *Mol. Biol. Cell* **16**, 2285–2300 (2005).
58. Yokogawa, T., Kitamura, Y., Nakamura, D., Ohno, S. & Nishikawa, K. Optimization of the hybridization-based method for purification of thermostable tRNAs in the presence of tetraalkylammonium salts. *Nucleic Acids Res.* **38**, e89 (2010).
59. Cheon, S. A. et al. Unique evolution of the UPR pathway with a novel bZIP transcription factor, Hx11, for controlling pathogenicity of *Cryptococcus neoformans*. *PLoS Pathog.* **7**, e1002177 (2011).
60. Jain, R. et al. RIP-Chip analysis: RNA-Binding Protein Immunoprecipitation-Microarray (Chip) Profiling. *Methods Mol. Biol.* **703**, 247–263 (2011).
61. Perez-Riverol, Y. et al. The PRIDE database and related tools and resources in 2019: improving support for quantification data. *Nucleic Acids Res.* **47**, D442–d450 (2019).

## Acknowledgements

We thank Professor Yong-Sun Bahn (Yonsei University, Seoul, Korea) for sharing *C. neoformans* strains, Professor Minhong Song (Chungnam National University, Daejeon, Korea) for sharing TPC-1 cells, and

Hyong Woo Choi (Andong National University, Andong, Korea) for helping and support with the SPR assay. This work was supported by the National Research Foundation of Korea (NRF) grant funded by the Korea government (MIST) (grant no.: 2021R1A2C2094730 to B.J., 2018R1A5A1025077 and 2021R1A2C3008934 to K.L., 2020R1A2C1005942 to H.K.K., RS-2024-00353152 to E.S., RS-2023-00248867 to Y.-H.K. and 2021R111A1A01054464 to Y. Hahn), the National Natural Science Foundation of China (grant no.:82260588 to H.J.), the Technology Development Program (20255915 to K.L.) funded by the Ministry of SMEs and Startups (MSS, Korea), and a grant of the Korea Health Technology R&D Project through the Korea Health Industry Development Institute (KHIDI), funded by the Ministry of Health & Welfare, Republic of Korea (grant no.: RS-2024-00339270 to K.L.).

## Author contributions

H.J., J.-H.Y., E.S., Y.Ha, H.L., D.K., M.J., Y.-H.K., H.K.K., M.R., H.-M.K. contributed equally to this work. H.J., J.-H.Y., and E.S. collected the data, developed experiments, interpreted the data, and organized the manuscript. M.J., H.J., D.K., and H.L. designed and performed in vivo and in vitro experiments. Y.-H.K. conducted tandem mass spectrometry analysis. D.K., H.-M.K., and Y.Ha performed northern blotting and primer extension assays. M.R. performed EMSA and SPR assay. H.K.K., J.K., and K.P.K. analysed data and revised the manuscript. Y.Hahn performed bioinformatic analyses of small RNA sequencing and total transcriptome data. J.B. and K.L. conceived idea, planned the project, supervised the study, interpreted data, and wrote the manuscript. All authors read and approved the manuscript.

## Competing interests

J.-H.Y., M.J., M.R., and H.-M.K. are employees of NES Biotechnology. J.-H.Y., H.-M.K., M.J., E.S., Y.Ha, M.R., K.L., and J.B. are inventors of KR Patent (Application No. 10-2022-00184521) entitled 'Anticancer Composition Containing Nanoparticle-tRH Conjugate'. K.L. is an inventor of US Patent (Patent No. US 8871509 B2) entitled "Nanoparticle-based gene delivery systems". The remaining authors have no conflicts of interest to declare.

## Additional information

**Supplementary information** The online version contains supplementary material available at <https://doi.org/10.1038/s41467-024-53624-4>.

**Correspondence** and requests for materials should be addressed to Jeehyeon Bae or Kangseok Lee.

**Peer review information** *Nature Communications* thanks the anonymous reviewers for their contribution to the peer review of this work. A peer review file is available.

**Reprints and permissions information** is available at <http://www.nature.com/reprints>

**Publisher's note** Springer Nature remains neutral with regard to jurisdictional claims in published maps and institutional affiliations.

**Open Access** This article is licensed under a Creative Commons Attribution-NonCommercial-NoDerivatives 4.0 International License, which permits any non-commercial use, sharing, distribution and reproduction in any medium or format, as long as you give appropriate credit to the original author(s) and the source, provide a link to the Creative Commons licence, and indicate if you modified the licensed material. You do not have permission under this licence to share adapted material derived from this article or parts of it. The images or other third party material in this article are included in the article's Creative Commons licence, unless indicated otherwise in a credit line to the material. If material is not included in the article's Creative Commons licence and your intended use is not permitted by statutory regulation or exceeds the permitted use, you will need to obtain permission directly from the copyright holder. To view a copy of this licence, visit <http://creativecommons.org/licenses/by-nc-nd/4.0/>.

© The Author(s) 2024